

Profiling quantum circuits for their efficient execution on single- and multi-core architectures

Medina Bandic^{1,3}, Pablo le Henaff^{1,3}, Anabel Ovide², Pau Escofet⁴, Sahar Ben Rached⁴, Santiago Rodrigo⁴, Hans van Someren¹, Sergi Abadal⁴, Eduard Alarcón⁴, Carmen G. Almudever², Sebastian Feld^{1,3}

Delft University of Technology, The Netherlands¹

Universitat Politècnica de València, Spain²

QuTech, The Netherlands³

Universitat Politècnica de Catalunya, Spain⁴

Abstract. Application-specific quantum computers offer the most efficient means to tackle problems intractable by classical computers. Realizing these architectures necessitates a deep understanding of quantum circuit properties and their relationship to execution outcomes on quantum devices. Our study aims to perform for the first time a rigorous examination of quantum circuits by introducing graph theory-based metrics extracted from their qubit interaction graph and gate dependency graph alongside conventional parameters describing the circuit itself. This methodology facilitates a comprehensive analysis and clustering of quantum circuits. Furthermore, it uncovers a connection between parameters rooted in both qubit interaction and gate dependency graphs, and the performance metrics for quantum circuit mapping, across a range of established quantum device and mapping configurations. Among the various device configurations, we particularly emphasize modular (i.e., multi-core) quantum computing architectures due to their high potential as a viable solution for quantum device scalability. This thorough analysis will help us to: i) identify key attributes of quantum circuits that affect the quantum circuit mapping performance metrics; ii) predict the performance on a specific chip for similar circuit structures; iii) determine preferable combinations of mapping techniques and hardware setups for specific circuits; and iv) define representative benchmark sets by clustering similarly structured circuits.

Keywords: Quantum circuit mapping, Multi-core quantum computers, Modular architectures, Quantum communication, Interaction graphs, Quantum benchmarks, Gate-dependency graphs

1. Introduction

In recent decades, the realm of quantum technology has witnessed remarkable progress, holding the potential to tackle problems that were once deemed insurmountable using classical means. Although these advancements are impressive, we are still in the early stages of understanding its full potential. The current generation of quantum devices, referred to as Noisy Intermediate-Scale Quantum (NISQ) devices [1], present severe limitations due to their size and susceptibility to noise. As a result, they are currently adept at handling only simple and modestly-sized circuits (i.e., executable descriptions of algorithms). These devices also face other hurdles, including restricted qubit connectivity, a narrow set of supported operations, and challenges pertaining to classical control resources [2, 3]. These collective constraints make the successful execution of a quantum circuit on such processors an intricate endeavor. Furthermore, NISQ devices often adhere to a ‘one-size-fits-all’ approach, which can lead to architectures ill-suited for certain quantum algorithms, resulting in lower success rates and fidelity. This is already well showcased in classical computing, where devices are often tailored for the purpose of usage (e.g., GPUs for gaming).

Most current quantum computers operate as single-processor devices, containing all qubits on a single chip. Scaling these designs proves challenging due to issues like crosstalk and limitations in control electronics [4]. An alternative approach, akin to classical computing, involves multi-processor (or multi-core) architectures, which are proposed by various quantum processor manufacturers [5–10]. These new designs facilitate distributed quantum computing that enables the execution of large algorithms across multiple cores to accommodate more qubits than a single processor can handle, and represent a feasible avenue for achieving scalability in quantum computing.

For both NISQ and multi-core architectures, the quantum circuit mapping process [11, 12] is necessary to efficiently run the circuits and maximize the usage of hardware resources. Quantum circuit mapping essentially represents adapting quantum circuits to quantum devices to adhere to all hardware constraints, forming a vital component of a full-stack quantum computing system [13].

Several studies emphasize the importance of considering a broader range of circuit features during the process of mapping [14–17]. A comprehensive profiling or characterization of quantum circuits offers several advantages, including gaining a better understanding of why certain algorithms achieve higher fidelity with specific processors and mapping techniques [18]. Additionally, it enables the classification and prediction of the performance of similar circuits based on the circuits’ attributes (like in [19]), all without the need for actual hardware execution. Moreover, this approach facilitates the development of mapping techniques and overall quantum systems customized for specific applications, respecting both the requirements (i.e., characteristics) of those particular circuits and the limitations of the hardware [13, 20, 21]; this consequently leads to an improvement in quality and execution time of solving currently intractable problems. It is important to note that this exhaustive characterization of quantum

circuits is not only the key for formulating meaningful and representative sets of quantum benchmarks that evaluate quantum circuit mapping techniques and entire quantum computing systems [22, 23], but also for establishing a suite of algorithm-level metrics to measure system performance [24].

The state-of-the-art characterization of quantum circuits proposed in [18] extends beyond conventional metrics such as qubit and gate counts. In addition to these standard attributes, their approach includes an examination of qubit interaction graphs, drawing insights from graph theory and machine learning to clarify the circuit’s two-qubit gate connections (qubit interactions). They performed an analysis of how these circuit parameters affect the performance of a specific quantum circuit technique when considering three different single-core devices.

In this paper, we extend the results of [18] by additionally encompassing metrics extracted from *gate dependency graphs* (which portray inter-dependencies among gates within the circuit), as well as parameters that describe the *density of the circuit* and its *repetitive oracles*. Furthermore, we not only consider parameters that are relevant for single-processor devices but also identify those that are of special interest for the next generation of *multi-core* architectures. Within our approach, we also experiment with *diverse quantum circuit mapping configurations* (four for single- and three for multi-core quantum architectures). This intricate exploration allows us to: i) discern the most influential quantum circuit attributes that impact the performance of circuit mapping; ii) predict the mapping performance of similarly structured quantum circuits on a specific chip; iii) identify the most adequate combination of mapping technique and quantum hardware for a given quantum circuit or set of circuits; and iv) define a representative benchmark set [24], by specifying a finite amount of groups of similarly-structured circuits. This thorough analysis, therefore, holds the potential to contribute to the future co-design of compilation methodologies driven by algorithms and the evolution of quantum hardware.

In summary, the main contributions of this paper are:

- (i) Performing the most comprehensive profiling of quantum circuits by extracting: a) standard parameters (i.e., number of qubits and gates, two-qubit gate percentage and depth), metrics from the b) interaction graph (e.g., average node degree), and c) gate-dependency graph (e.g., critical path length), d) gate density related parameters (e.g., amount of idling) and e) characteristics related to repetitive sub-circuits. We believe that this list of parameters encompasses all relevant aspects of a quantum circuit. It helps us gain insights into why certain circuits excel or falter on particular architectures, potentially revealing correlations between circuit structure and performance across different quantum setups. Leveraging these parameters, we can adapt existing or craft new full-stack quantum systems with higher precision.
- (ii) Identifying, for the first time, circuit parameters that are key for scalable modular quantum computing architectures. Those architectures demand a unique parameter set due to their intricate quantum circuit mapping requirements, as elaborated in

detail in Sec. 2.

- (iii) Finding a correlation between extracted circuit features and compilation performance across various mapper-device combinations for single-core and multi-core architectures (totaling in seven mappers and six devices). Utilizing the Pearson correlation score [25], we rank parameters from most positively correlated to most negatively correlated for each combination. This analysis shows the significance of selecting suitable device topologies and mapping techniques for quantum circuits with specific structural parameters. It also highlights the key circuit parameters crucial for designing application-aware quantum systems. Identifying these influential circuit parameters marks the initial stride towards crafting such systems.
- (iv) Clustering similarly structured circuits and determining the most effective mapper-device setups for them. We illustrate how these clusters also correspond to circuit origin groups found in qbench (i.e., random, QUEKO, real algorithms) [22]. This discovery of distinct groups of quantum circuits allows us to establish representative sets of quantum benchmarks without the need for an exhaustive list, which also facilitates the design of application-specific quantum systems tailored to each group, rather than a separate system for each benchmark.

The paper is organized as follows: Sec. 2 introduces single- and multi-core computation and quantum circuit mapping, as well as the previous work on quantum circuit characterization. Sec. 3 showcases our novel circuit parameters and profiling process in this work, done for single- and multi-core quantum computation separately. In Sec. 4, we dive into methodology and performance metrics. We show and discuss results in Sec. 5 and finally conclude our work in Sec. 6.

2. Background and previous research

2.1. Multi-core quantum computation

Just like for classical computing, modular architectures are envisioned as a solution for the scalability of quantum devices and they are expected to accommodate thousands to millions of qubits within a single system. For dealing with problems regarding crosstalk, classical control electronics, and wiring complexity, qubits are distributed over multiple cores or processors. This strategy capitalizes on quantum parallelization while addressing qubit control demands and improving qubit isolation [26]. Nevertheless, constructing multi-core processors introduces new challenges, mainly due to latency-prone quantum communications that introduce inefficiencies. Quantum state transfer across chip-scale networks represents an alternative to conventional communication technologies, which prove impractical for modular architectures. Communication latencies heighten the risk of data loss during qubit transmission due to state decoherence [2]. Several strategies have emerged to create inter-core communication networks for modular quantum computing architectures, accommodating varying technology

platforms. These include quantum links for superconducting chips [27], ion-shuttling for ion-trapped quantum computers [28], and photonic networks [29]. Modularity requirements extend beyond the qubit layer, imposing constraints on networking, control, and compilation layers, necessitating a comprehensive software-hardware stack [26].

2.2. The quantum circuit mapping problem

As previously stated, running a quantum circuit on any device is not a straightforward task. Given the constraints of current NISQ devices (e.g., highly error-prone and limited size and qubit connectivity), the execution of quantum circuits often requires making some modifications within the circuit. This process, referred to as quantum circuit mapping, is pivotal in adapting algorithms to quantum devices, and it forms a vital component of a full-stack quantum computing system [30]. Limited connectivity is the main challenge addressed by quantum circuit mapping because, during the execution of circuits, all interacting logical/virtual qubits (of the circuit) must be adjacent. This problem is solved by finding the most suitable allocation of logical qubits to physical qubits on the chip, and repositioning those logical qubits on the chip to make them adjacent when necessary, which is usually done by inserting additional gates (e.g., SWAPs or shuttle operations). The specifics of quantum circuit mapping can differ from one device to another due to technology disparities and qubit connectivity. Ensuring effective utilization of limited hardware resources and minimizing errors during quantum operation execution by reducing additional gates and circuit latency necessitates this process. Yet, solving the quantum circuit mapping problem as the qubit count increases is computationally challenging, even for current monolithic (or single-core) devices. To address this, diverse quantum circuit mapping algorithms have been introduced, ranging from heuristic and brute-force strategies to graph-theoretical techniques, dynamic programming algorithms, and machine learning-based approaches [17, 31–54], relying on different performance metrics like gate count, circuit depth (i.e., number of layers of gates where gates can run in parallel), fidelity [39, 40, 55] or the circuit success rate [36, 56].

However, mapping techniques designed for single-processor NISQ devices do not readily apply to modular multi-core (or multi-node) quantum computing architectures, which offer a promising path for quantum computing scalability [2]. This architectural approach involves cores (quantum processing units, or QPUs) interconnected via classical and, ultimately, quantum communication channels. Quantum links facilitate the transfer of quantum states among processors or the execution of inter-core quantum gates depending on the technology, while classical links ensure the coordination of quantum communication [57]. The intricate communication channels and traffic patterns in multi-core architectures add complexity to quantum circuit mapping compared to single-core devices [3, 58, 59]. In response, novel techniques have emerged for modular architectures, aiming to minimize the costly (in terms of time and effort overhead or reduced fidelity) long-distance inter-core operations. To reduce the amount

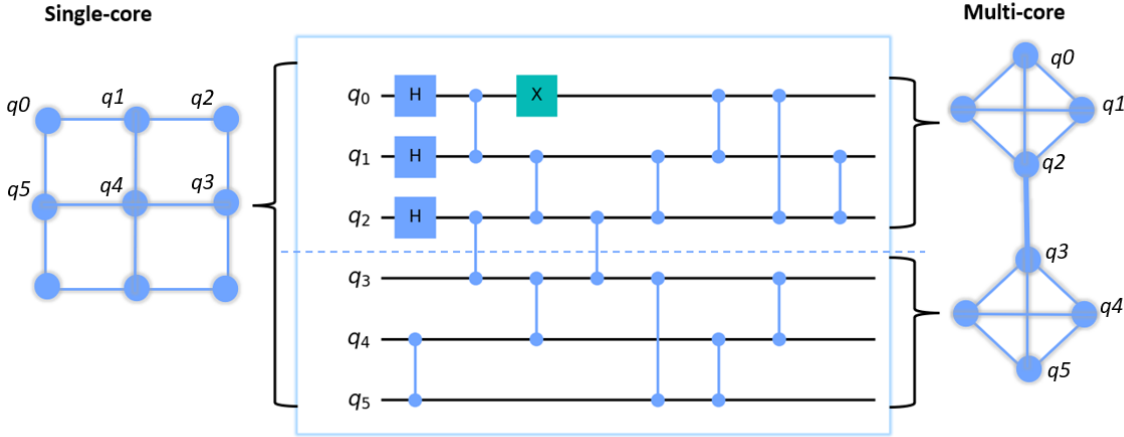


Figure 1: Initial mapping of a quantum circuit (middle) to a single-core (left) or multi-core device (right); For the latter case, the quantum circuit is partitioned into two highly connected circuit slices so that any communication between the two cores is minimized.

of inter-core operations, it is essential to efficiently allocate logical qubits across the physical qubits of the given cores. While the literature in this emerging domain is limited, some approaches have concentrated on quantum compilation and mapping for modular quantum computing [60–63]. In these approaches, the quantum circuit is divided into smaller partitions, and interaction graphs reflecting operations within a circuit segment are mapped onto cores by grouping qubits with high interaction levels (see Fig. 1).

All previously stated strategies within both single- and multi-core quantum computation share a common goal: tailoring quantum circuits to device-specific attributes and constraints, while minimizing the communication overhead. However, they often only focus on a limited set of circuit features, such as gate and qubit counts, and qubit interactions. What is missing is a more comprehensive quantum circuit characterization that goes into deeper aspects. For example, one can explore the characteristics of the qubit interaction graph, such as the frequency of interactions between qubit pairs [18] and the distribution of these interactions among qubits, as well as the quantum instruction dependency graph (representing gate dependencies for scheduling).

Some researchers have already highlighted the significance of incorporating application-specific properties [13, 15–18, 37] to enhance quantum circuit mapping and overall quantum system performance. Even in classical computing, the allocation of computing resources depends on the intended applications and processes. In a similar vein, thorough profiling aids in identifying the essential circuit features for successful execution on a particular device and vice versa. Yet, as we explore the intricacies of running algorithms on modular architectures, it becomes evident that this realm demands a distinct approach when compared to conventional monolithic NISQ devices.

Consequently, profiling quantum circuits in the context of modular architectures should adopt a tailored strategy and select parameters that align with the nuances of this scenario.

In conclusion, understanding the structural attributes of quantum circuits sheds light on why and which groups of algorithms perform better on specific processors with designated mapping techniques than on others. This holistic understanding not only guides mapping but also opens avenues for improving the overall performance of quantum circuits on quantum hardware and represents a first step towards application-based quantum computers.

2.3. On the importance of qubit interaction and gate-dependency graphs

Quantum circuits so far have mostly been characterized in terms of size, i.e., the number of qubits, gates, two-qubit gates, and depth, which are blind to the circuit's structure. Considering that the main quantum hardware constraints are low fidelity and limited qubit connectivity, it is important to extract more information about the qubit interaction distribution as well as gate dependencies as they directly relate to gate and depth overhead that results from the compilation process. Previous works have emphasized the significance of deriving additional circuit parameters based on qubit interaction and quantum instruction dependency graphs for the development of mapping techniques [12, 32, 33, 62]. While gate dependency graphs have been utilized for operation scheduling optimization and look-ahead techniques, interaction graphs have typically been employed for the initial qubit placement and routing procedure. In this work, we utilize these two graphs and their graph-theory-based attributes for characterizing circuits targeting both single- and multi-core architectures. In the next paragraphs, we will introduce these two graph representations of the quantum circuit.

The *Interaction Graph* (IG) $G_i(V_i, E_i)$ offers a visual representation of the spatial distribution of two-qubit gates for a given quantum circuit. Typically, this is an undirected and connected graph (see Fig. 2(b)), with edges denoted as $e(v_i, v_j) \in E_i$ representing the two-qubit gates and nodes labeled as $v_i \in V_i$ representing the qubits engaged in these gates [18, 62]. Previous research [18] has demonstrated that different categories of circuits (e.g., real algorithms and random circuits) exhibit varying compilation performance in terms of gate and depth overhead as well as fidelity decrease when executed on different physical-qubit topologies (see Figs. 5 and 14 of [18]). To understand the underlying reasons for these differences, prior studies have explored the structural disparities between various quantum circuit groups based on their interaction graphs. The quantum circuit mapping problem can be conceptualized as a graph problem, in which the comparison between the interaction graphs of a circuit and the coupling graph of the device is crucial [54]. Therefore, the parameters of the interaction graph can significantly influence the outcome. Studies such as [18, 24] have illustrated how the interaction graph and size parameters of quantum circuits directly correlate to their performance on different chips when employing the same mapping technique.

For example, circuits with fully connected interaction graphs are expected to incur higher overhead, unless the processor’s coupling graph is fully or almost fully connected. Moreover, research such as [18] has further clustered the circuits based on these extracted parameters and identified performance discrepancies among the groups based on the aforementioned mapping metrics.

Interaction graphs play an even more significant role in the compilation of circuits for multi-core systems [64]. Mapping to multi-core devices involves minimizing inter-core communication by partitioning the interaction graphs and effectively allocating the logical qubits (IG nodes) onto the physical qubits of different cores. This is achieved by aiming to map highly interacting qubits (with high IG weights) onto the same core. Given the importance of IG partitioning in modular compilation and its distinct approach compared to single-core systems, it is essential to use different IG metrics. These metrics should focus on identifying local clusters and cliques to effectively describe how ‘partitionable’ a circuit is.

Besides that, the *Gate-Dependency Graph* (GDG) $G_{gd}(V_{GD}, E_{GD})$ is a directed and connected graph illustrating the interrelations between the gates in the circuit. Each gate in the circuit is represented by a node $v_j \in V_{GD}$, and the dependency between gates is depicted as a directed edge $e(v_j, v_k) \in E_{GD}$. An illustrative example of this concept is shown in Fig. 2, where a quantum circuit consisting of 6 qubits and 8 two-qubit gates is displayed alongside its corresponding IG and GDG [43]. It is worth noting that both graphs can also be represented as weighted graphs: the IG becomes weighted when multiple two-qubit operations occur between the same pairs of qubits, while the GDG becomes weighted when considering, for instance, gate duration (i.e. time). For the purpose of this paper, we focus on the simplified, unweighted version of GDG, where all gates take one time step.

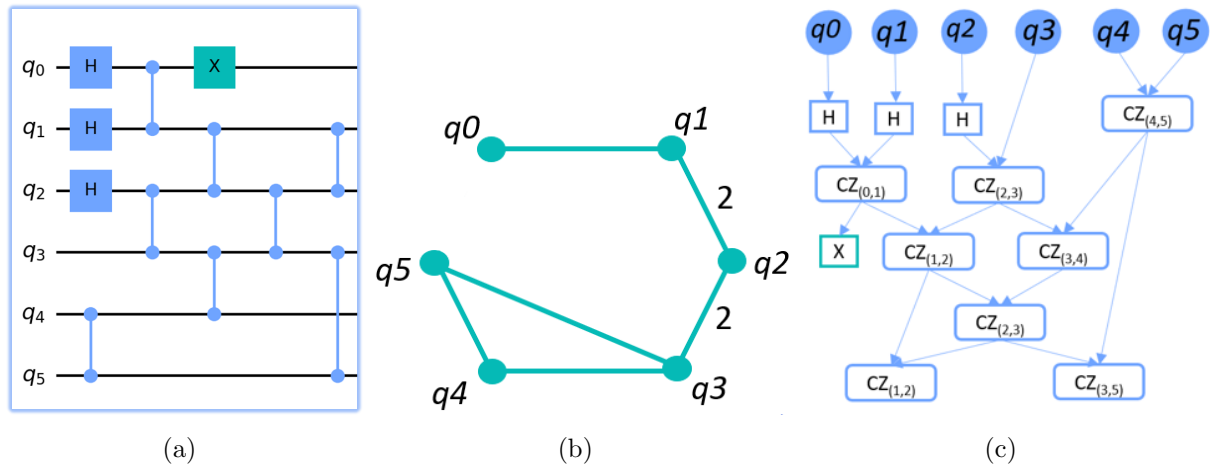


Figure 2: An exemplary quantum circuit (a) and its corresponding qubit interaction graph (b) and gate dependency graph (c).

In this paper, we aim to examine quantum circuits by analyzing parameters

extracted from interaction graphs that are relevant for single- and multi-processor architectures, from gate dependency graphs (e.g., path distribution and critical path length), parameters related to repeating sub-circuits/oracles within the circuit, and circuit density-related parameters, followed by a clustering of the circuits. Our focus is to identify and quantify the relationships between circuit parameters, clusters, and various compilation techniques across different quantum topologies. Gaining a comprehensive understanding of circuit structures can aid in designing quantum systems optimized for the highest success rates for specific circuit groups and help define a finite set of representative benchmarks.

In the subsequent sections, we will provide a detailed overview of the entire quantum circuit profiling process.

3. Characterizing quantum circuits – definition and profiling

3.1. Parameter selection

Tab. 1 illustrates the five groups of circuit parameters we consider in this work. The process selection of the **parameters of interest** involved two steps: 1) Selecting parameters within these groups relevant to single- and multi-core architectures considering their main constraints. For instance, the clustering coefficient [65] is important for the execution of circuits in multi-core devices but not in single-core devices, as it requires graph partitioning. Conversely, node degree is relevant to both scenarios: a higher average degree in the interaction graph makes mapping more challenging; and 2) Reducing the number of parameters by identifying highly correlated ones using the Pearson correlation matrix [25], like in [18].

The resulting reduced set of parameters is as follows [18,65]:

3.1.1. Size Standard parameters used for circuits description in previous works:

- *Number of qubits:* n_q
- *Number of gates:* n_g
- *Two-qubit gate percentage:* $\frac{n_{2qg}}{n_g}$, where n_{2qg} is the number of two-qubit gates.
- *Decomposed circuit depth:* d

3.1.2. IG (definitions taken from [18])

- *Average shortest path length:* Average hopcount between all nodes [65]. The larger the average hopcount between the nodes, the less connected the graph is. It also means that a simpler interaction graph is easier to map.
- *Standard deviation of adjacency matrix* $\sigma(A)$: An adjacency matrix A is a square matrix used for representing a graph whose elements are $a_{ij} = a_{ji}$ represent the number of connections between nodes n_i and n_j . It shows which nodes are connected and with how many edges. A large σ value means some specific pairs of qubits interact much more than others and that there is less additional routing required.

- *Diameter*: Longest shortest path in the circuit,

$$dm = \max_{n_i \in \mathcal{N}}(\epsilon_i),$$

where ϵ_i is the longest hopcount between node n_i and any other node among the total of N nodes. The larger the diameter, the simpler the IG and, therefore, easier to map onto a device.

- *Central point of dominance*: Maximal betweenness of any node in the graph, where betweenness is the number of shortest paths between nodes that traverse some node or edge [65]. A value of 0 results for complete graphs, and 1 for star-shaped graphs. Values approaching 0 or 1 are undesirable from the perspective of quantum circuit mapping, as 0 reports a graph that is too much connected, and 1 indicates that one qubit is involved in all gates, making the circuit hard to parallelize.
- *Average degree*: Average degree of neighbor nodes, where the degree is the number of nodes to which one node is connected and defined as

$$deg_i = \sum_{j=1}^N a_{ij}.$$

The lower the value of the average degree, the less connected the IG is, and the easier it is to map.

- *Number of maximal cliques*: The total number of the largest all-to-all connected subgraphs. This metric also depends on the size of the maximal clique. The smaller the largest clique, the less connected the graph and, therefore, easier to map. Another cliques-related graph metric is *clustering coefficient* which measures the cliquishness of a neighborhood. The values range between 0 and 1, where 1 represents a fully connected graph, which is always the worst-case scenario for the quantum circuit mapping:

$$c_i = \frac{y_i}{\binom{deg_i}{2}},$$

where y_i is the number of links between neighbors of node n_i . These two metrics are of high importance for multi-core computation as they show the presence of highly connected clusters of nodes within the graph, which is related to the IG partitioning part of multi-core quantum circuit mapping.

- *Vertex/edge reliability*: The minimal number of nodes/edges whose removal can disconnect the graph. The lower the reliability, the easier it is to partition the graph for multi-core mapping.
- *Coreness*: Maximal k for specific node i such that i is present in k -core graph but removed from $(k+1)$ -core (k -core is a subgraph of some graph made by removing all the nodes of degree $\leq k$). Coreness as the local metrics also relates to IG partitioning and modular computing.

- *Pagerank*: Ranking of the importance of each node in the graph [66] based on the number and weights of the links with other nodes and the rank of those nodes. This graph metric emphasizes which nodes should be mapped to the most connected part of the chip.

3.1.3. GDG One of the main disadvantages of current QPUs is the short lifetime of qubits, i.e., their decoherence. That makes the circuit *scheduling* one of the crucial segments of the quantum circuit compilation. The goal during scheduling is to make the gates run as parallel as possible. However, not every circuit is parallelizable. GDG and especially its *critical path* (longest path in GDG) showcases the minimal necessary duration of the circuit and represents its longest inter-depending gate sequence. Therefore, this sequence of gates should be scheduled to run as soon as possible in order to shorten the circuit duration and prevent qubit decoherence. Metrics related to critical and other paths of GDG can also tell us how sequential the circuit is and, therefore, how easy it is to map to a single or to multiple cores. Qubits participating in the inter-dependent gates (gates of the same common paths) should be placed nearby on a chip or within the same core during the mapping process. Furthermore, the higher the percentage of the circuit gates included in the critical path, the more sequential the circuit is and, therefore, less parallelizable. Metrics that describe the GDG paths include:

- *Critical path length* or number of gates in the critical path;
- *Number of critical paths*;
- *Path length distribution* and its mean and standard deviation; and
- *Percentage of gates included in the critical path*.

These metrics' implementation and detailed definitions are shown in Appendix B.

3.1.4. Circuit density This set of metrics evaluates the degree of parallelization of the circuit gates before any optimizations. It indicates the number of gates executed in each layer (time-step) of the circuit relative to the maximum number of gates that could be executed if the circuit were fully parallelized (similar to Quantum Volume circuits [56]). A denser circuit implies greater difficulty in further optimization and execution. This paper utilizes two metrics to describe this behavior:

- *Density score*: Parallelization level of the circuit;

$$D = \frac{\frac{2*n_{2qg}+n_{1qg}}{d} - 1}{n_q - 1},$$

where n_{2qg} and n_{1qg} are number of two- and single-qubit gates, respectively. This is an extended version of the parallelism metric from [24]: we made a distinction between the single- and two-qubit gates for better preciseness, where D can actually reach all the values in the range between 0 and 1, (1 is maximal density); and

- Idling score: Average amount of qubit idling in the circuit;

$$I = \frac{\sum_{i=1}^{n_q} d - q_i}{n_q * d},$$

where q_i signifies the number of layers of the circuit in which the qubit is used; range between 0 and 1, with 0 meaning no idling and 1 meaning no scheduled gates.

3.1.5. Longest sub-circuit repetitions In circuits that are based on real algorithms, there are always patterns in terms of gate order and repetitions. In contrast, completely random circuits show, on average, no such patterns. In order to express the randomness of the gates and groups of gates in circuits, we have defined the following metrics

- The number of occurrences of the largest repetitive sub-circuit; and
- The size of this largest repetitive sub-circuit.

The extraction of these two metrics relies on existing algorithms used for strings of characters. The problem of finding the longest repeating sub-string in a text and the length thereof is efficiently solved by filling a data structure called a *suffix tree* [67]. We used the same implementation by identifying characters and quantum gates. The significance of gate randomness on circuit performance is closely tied to the type of mapper employed. Some mappers are expected to exhibit a high correlation, where the routing algorithm is designed to identify gate patterns in advance. In contrast, more stochastic approaches do not benefit from recognizing these patterns.

The IG parameters reveal patterns necessary for initial placement algorithms, whereas GDG parameters indicate the length and sequential nature of the circuit, crucial for mitigating decoherence and enhancing scheduling and routing. Parameters related to circuit density illustrate the extent of parallelization in the circuit before optimization, influencing the complexity of all stages of quantum circuit mapping. Additionally, identifying recurring gate patterns in the circuits assists in refining scheduling and look-ahead routing techniques. For the complete list of metrics, please refer to [11] (IG-based) and Appendix D and Appendix C.

3.2. Quantum circuit clustering

As previously stated, one of our objectives is to identify structural similarities among quantum circuits and establish “circuit families”, wherein the constituent elements (i.e., the quantum circuits) exhibit similar compilation behavior and require comparable hardware resources. For this purpose, we employed a two-step clustering approach: an initial clustering of circuits based on size parameters (Group 1), followed by clustering based on the remaining parameters. This strategy was implemented to prevent size parameters from exerting undue influence on the clustering algorithm. Consequently, we initially categorized the set of 341 selected benchmarks (see Sec. 4) into five clusters using the K-means clustering algorithm [68]. Subsequently, each of the five size-related clusters could be further subdivided into sub-clusters based on the previously described

Table 1: Selected metrics for the characterization of quantum circuits.

Metric	Metric Type	Single- or Multi-core
Num. of qubits	Size	Both
Num. of gates	Size	Both
Two-qubit gate %	Size	Both
Circuit depth	Size	Both
Avg. shortest path	IG	Single-core
Standard deviation of adjacency matrix	IG	Single-core
Diameter	IG	Multi-core
Central point of dominance	IG	Multi-core
Maximal cliques and num. of maximal cliques	IG	Multi-core
Clustering coefficient	IG	Multi-core
Avg. degree	IG	Both
Vertex/edge reliability	IG	Multi-core
Coreness	IG	Multi-core
Pagerank	IG	Multi-core
Critical path length	GDG	Both
Num. of critical paths	GDG	Both
GDG path length distribution metrics	GDG	Both
% of gates in critical path	GDG	Both
Density score	Circuit density	Both
Idling score	Circuit density	Both
Num. of largest rep. sub-circuit	Sub-circuit repetitions	Both
Size of largest rep. sub-circuit	Sub-circuit repetitions	Both

structural circuit parameters (groups 2-5). In this regard, we once again opted for the K-means algorithm after evaluating various methods and parameter configurations using the silhouette coefficient method [69]. The specific settings for clustering single- and multi-core devices, as well as the clusters themselves, are detailed or referred to in Appendix C and Appendix D, respectively. It is expected that circuits assigned to the same sub-cluster will exhibit similar fidelity and gate overhead outcomes. The correlation between our circuit groups and mapping performance metrics, as well as potential explanations for these relationships, will be discussed in the subsequent sections.

4. Methodology

In our research, the quantum circuit profiling process encompasses the following four steps:

- (i) **Benchmark collection** – We gather benchmarks (i.e., quantum circuits) from

diverse sources, translate them into the same quantum language (in our case cQASM [70]), and extract their interaction and gate-dependency graphs [18].

- (ii) **Parameter selection and extraction** – We select and extract graph-theory-based parameters from the qubit interaction graph and gate dependency graph, focusing on parameters relevant to mapping quantum circuits to single-core and multi-core devices. Additionally, we extract supplementary circuit parameters to enhance the characterization related to circuit density.
- (iii) **Benchmark clustering** – We cluster benchmarks based on their size-related (number of qubits and gates, two-qubit gate percentage, and circuit depth) and structure-related parameters.
- (iv) **Compilation** – We compile the quantum circuits using Qiskit [71], OpenQl [72], and additional multi-core compilation solutions [62,63], and analyze the relationship between their performance and the extracted parameters, as well as their cluster affiliation (see Sec. 5).

4.1. Quantum benchmarks selection

In this paper, we employed the qbench benchmark set [18, 22], which offers a comprehensive collection of quantum circuits sourced from various platforms and written in different programming languages. This set encompasses a range of circuit types categorized based on their origin, including circuits derived from real quantum algorithms (e.g., QFT), simpler algorithm-based circuits (such as arithmetic circuits), QUEKO circuits optimized for specific devices [73], and randomly generated circuits produced by randomly selecting single- and two-qubit gates from a predefined set and applying them to arbitrarily chosen qubits or qubit pairs [74]. This category also includes highly parallelized Quantum Volume circuits used for device benchmarking [75].

Given the inclusion of multi-core architectures in our study, we also incorporated benchmarks used so far for multi-core computations [3, 12, 59, 62]. These benchmarks comprise a variety of circuit instances, ranging from 16 to 128 qubits, such as the Cuccaro Adder [76], Grover’s main routine, GHZ state preparation [77], QFT, QAOA, and VQE [78]. To accommodate this aspect, we expanded our synthetic circuit set to include instances with up to 128 qubits. The complete list of 341 quantum circuits utilized in our study is detailed in Appendix A, with accompanying code available at [22].

4.2. Hardware configuration

To investigate the relationship between the previously identified circuit clusters (see Sec. 3) and the mapping outcomes, we compiled the selected quantum circuits using various target single-core and multi-core quantum architectures. For single-core architectures, we utilized the *Rigetti Aspen-1*, *Surface-17* [33], *IBM Rochester*, and *Google Bristlecone* devices, as depicted in Fig. 3. Regarding modular architectures, we adopted the same configuration as detailed in [62]: all-to-all connected qubits within the cores, while

the cores themselves are interconnected either in an all-to-all manner or in a grid-like fashion, as illustrated in Fig. 4. These device configurations were selected because they are commonly employed in quantum circuit mapping research and offer realistic and diverse connectivity patterns in their coupling graphs. Note, that we did not execute the quantum circuits on actual devices; instead, the hardware constraints of the devices were considered during the compilation process alone.

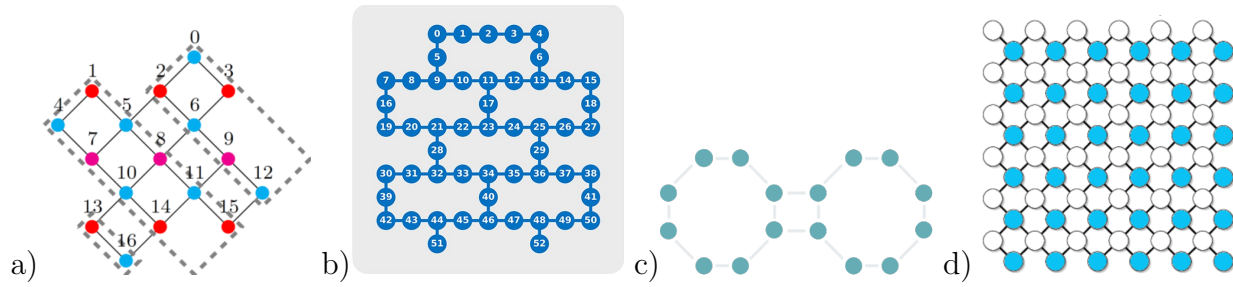


Figure 3: Topologies of the quantum architectures used in our experiments: a) Surface-17; b) IBM Rochester; c) Rigetti 16-q Aspen and d) Google Bristlecone. Figures and device configurations taken from: [33, 79–81].

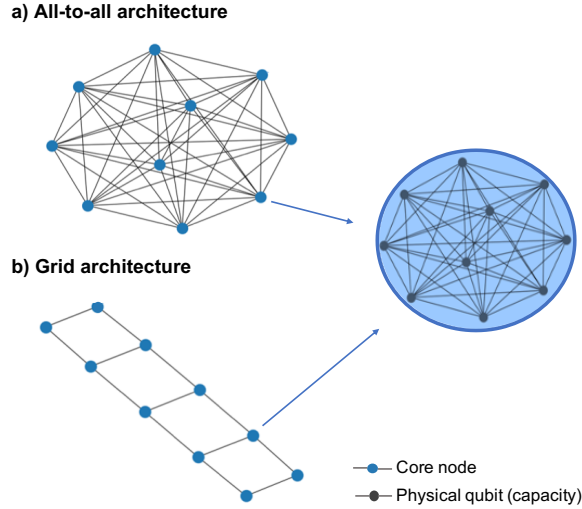


Figure 4: In our experiments, we examined two distinct multi-core architectures: **a)** All-to-all connected cores and **b)** 2D Grid core connectivity. Each node in the two graphs on the left represents a core, while the edges correspond to communication links between the cores. On the right, the intra-core qubit topology is displayed, comprising 10 all-to-all connected qubits. We chose these topologies due to their ability to offer a simplified representation of architectures anticipated to emerge in the near future. This approach enables us to promptly address the immediate need for mapping solutions based on minimizing inter-core communication before going into more complex architectures [62].

4.3. Quantum compilers

In this study, we investigate not only the relationship between different quantum circuit groups, parameters, and quantum devices but also explore the connection between quantum circuits and mapping techniques. The goal is to gain insights into developing and selecting mapping techniques tailored to circuits with specific common properties.

For single-core devices, we utilize the widely used Qiskit compiler and test four combinations of compilation settings by pairing two routers with two optimization levels. Specifically, we employ the *Stochastic* and *Sabre* routers, along with optimization levels 1 and 2. The key distinction between the Stochastic and Sabre approaches lies in their routing path selection: Sabre utilizes a more deterministic approach, whereas Stochastic employs a more randomized strategy. Optimization level 1 involves simplistic mapping with minimal circuit optimization but short runtime, while optimization level 2 employs more aggressive gate cancellation and commutation techniques to minimize qubit crosstalk and increase parallelism. Level 2 is suitable for complex circuits or cases in which circuit optimization is crucial despite requiring more computational resources and time during compilation. For simplicity, we will refer to these four method combinations as *Stochastic1*, *Stochastic2*, *Sabre1*, and *Sabre2*.

In the modular regime, we explore three techniques:

- The *time-sliced circuit partitioning* method [12], which leverages qubit clustering to create tractable partitioning heuristics for mapping quantum circuits to modular physical machines one slice at a time. This method also uses a tunable lookahead scheme to reduce the cost of moving to future time slices.
- The *Hungarian Qubit Assignment* (HQA) algorithm [63], which employs the Hungarian algorithm [82] to enhance qubit-to-core assignment by considering interactions between qubits across the entire circuit, and enabling fine-grained partitioning and enhanced qubit utilization.
- A *QUBO*-based approach [83], which encodes qubit allocation and inter-core communication costs in binary decision variables [62]. This method splits the quantum circuit into slices and formulates the qubit assignment as a graph partitioning problem for each slice, reducing costly inter-core communication by penalizing that. The final solution minimizes the overall cost across all circuit slices.

4.4. Performance metrics

Quantum circuit mapping performance metrics are defined as follows:

- (i) **Gate overhead** is calculated using the formula: $G_{\text{overhead}} = \frac{(G_{\text{after}} - G_{\text{before}})}{G_{\text{before}}}$. Here, G_{before} and G_{after} denote the number of gates before and after compilation, respectively.

- (ii) **Depth overhead** is determined by: $D_{overhead} = \frac{(D_{after} - D_{before})}{D_{before}}$, where D_{before} and D_{after} represent the circuit depth before and after compilation. Depth refers to the number of cycles or layers of simultaneously running gates in the circuit.
- (iii) **Fidelity decrease** is computed as: $F_{decrease} = \frac{(F_{before} - F_{after})}{F_{before}}$. Here, F_{before} and F_{after} represent the circuit fidelity before and after compilation, respectively. *Circuit fidelity* is a product of the error rates of the gates in the circuit. The primary objective during circuit mapping is to maximize this metric. We assumed uniform error rates for all one-qubit and two-qubit gates, using average values from the Starmon-5 chip [70, 84, 85].
- (iv) **Number of non-local (inter-core) communications** is the number of qubit moves from one core to another within modular quantum architectures. Entanglement-based quantum communication protocols are employed that require Bell-pair generations that enable the teleportation of quantum states. However, generating entangled pairs results in a resource overhead, and the process itself is non-deterministic, adding complexity to scheduling tasks [3].

In the following section, we will discuss the relation of the structural parameters of circuits from Sec. 4.1 with the above-stated obtained metrics after mapping them into different combinations of quantum system setups mentioned in Secs. 4.2 and 4.3.

5. Results and discussion

In this section, we assess and contrast the mapping results of our chosen circuits while examining the influence of circuit parameters on the outcomes. Furthermore, we juxtapose the performance of various circuit clusters using different mapping techniques and processor designs.

5.1. Mapping to single-core devices

We begin our analysis by examining the correlation between the circuit parameters introduced in Sec. 3 and the three quantum circuit mapping performance metrics across four different single-core architectures: Surface 17, IBM Rochester, Rigetti Aspen, and Google Bristlecone (see Fig. 3). The correlations are visualized in Fig. 5(a) using a Pearson correlation map, where the correlation values range from dark red for the highest positive correlation to dark blue for the highest negative correlation. A positive correlation means that if values of one parameter increase, then so do of the other, and a negative is vice versa. White color, and correlation factors around zero indicate no significant correlation. The parameters are sorted to facilitate the identification of the most correlated ones. Notably, while some parameters are consistently important across all devices and metrics, others are not significant (e.g., the number of gates), and some vary in importance depending on the metrics and devices (e.g., the number of qubits has a high negative correlation factor only for the fidelity decrease in the IBM Rochester device). In addition to the analysis of the four devices using the same

mapping technique (Sabre2), Fig. 5(a) also includes results for two different mapping configurations, namely Stochastic1 and Sabre2 (see Sec. 4.3), for the Google Bristlecone device. The configurations Stochastic2 and Sabre1 are not shown, as their correlation results are similar to Stochastic1 and Sabre2, respectively. This suggests that the routing technique is more significant than other optimization passes concerning different circuit parameters. For the same reason, we opted to use Sabre2 and Stochastic1 for the rest of the experiments explained in this section.

To investigate the meaning of these correlations, we plotted 3D graphs of some of the highest-correlated parameters. As examples, we selected: 1) the gate overhead metric for the Surface 17 device with parameters: average shortest path length, density score, and idling score, shown in Fig. 5(b), and 2) the depth overhead metric for the Rigetti Aspen device with circuit parameters: number of qubits, average IG degree, and number of critical paths, shown in Fig. 5(c). In Fig. 5(b), we observe that the average shortest path length and density score metrics are negatively correlated with the gate overhead, meaning that higher values of these metrics correspond to a lower gate overhead. Conversely, the idling score shows a positive correlation. This implies that a higher average shortest path length simplifies running the circuit due to a simpler interaction graph (IG), confirming our hypotheses in Sec. 3.1.2. In Fig. 5(c), the average degree of the IG is shown to be highly influential for the depth overhead: a higher degree indicates a denser IG, leading to a larger depth overhead. The number of qubits and the number of critical paths also exhibit positive correlations.

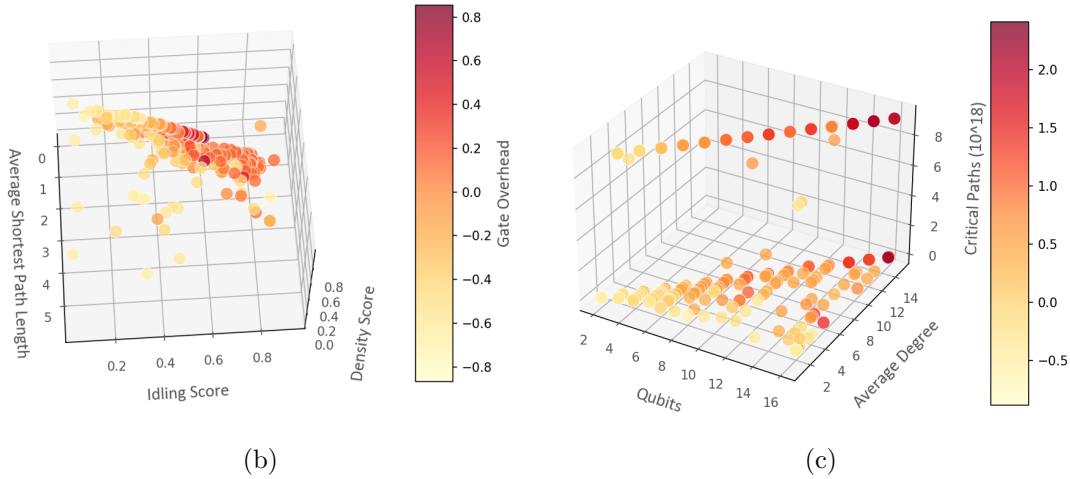
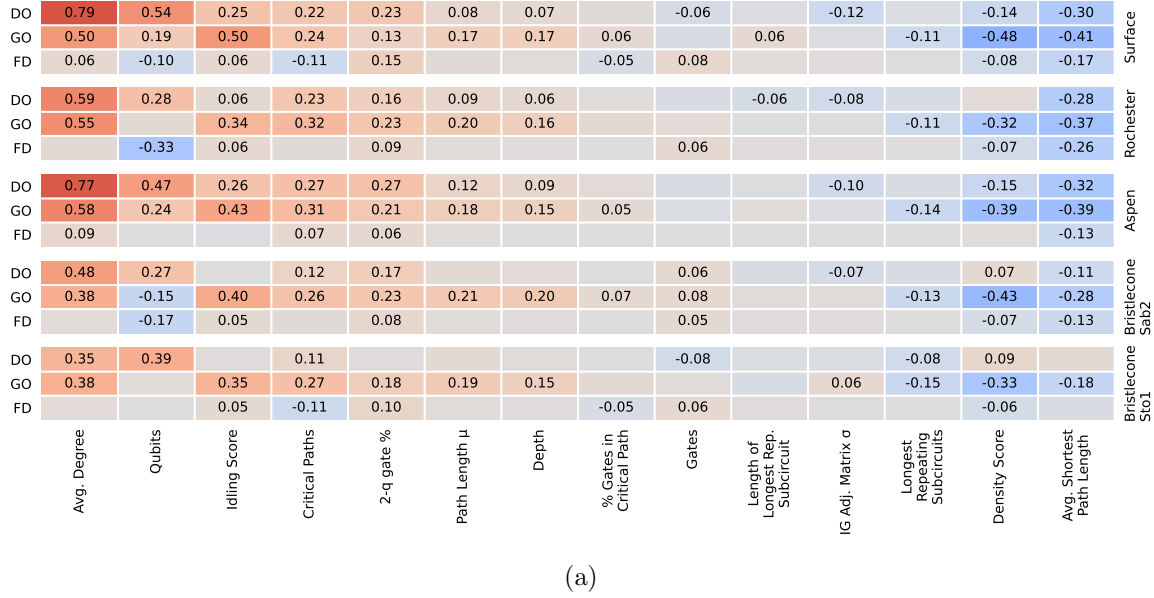


Figure 5: a) Correlation of the gate overhead, depth overhead and fidelity decrease compilation performance metrics with circuit parameters while using 4 different device configurations: Surface 17, IBM Rochester, Rigetti Aspen and Google Bristlecone for Sabre2 mapper, and Bristlecone device for Stochastic1 mapper. Metrics are ordered from the most positively correlated to the most negatively correlated one (red to blue). b) Three parameters with high performance correlation for the Surface 17 topology: idling score, density score and avg. shortest path length and their gate overhead. c) Three parameters with high performance correlation for the Aspen-16 topology: average degree, number of critical paths and number of qubits and their depth overhead.

In the next part of our work, we created “circuit families” containing circuits of similar structure based on extracted features. The two-level clustering approach used to achieve this is explained in Sec. 3.2. Fig. 6 presents examples of these created families and their results concerning the three compilation metrics. Figs. 6(a), 6(b) and 6(c) illustrate performance differences when targeting Surface 17, Bristlecone using

Sabre2 mapper, and Bristlecone using the Stochastic1 mapper, respectively. Notably, the group of circuits marked in purple (Group 0) performed better on average with Bristlecone than on Surface 17, exhibiting approximately 20% fewer gates. Conversely, the group noted in grey (Group 5) performed better on Surface 17, particularly in terms of fidelity decrease, which remained below 40% except for one outlier. In contrast, for the Bristlecone device, the majority of benchmarks for this group ranged between 60% and 100%. The Stochastic1 mapper generally performed worse than Sabre2, as expected due to its simplicity. For example, Group 3 (yellow) reached 150% in gate overhead, and Group 5 reached 200% in depth overhead, whereas these metrics for Sabre2 were 75% and 150%, respectively. However, Group 0 did not show significant performance differences between the two mappers, with benchmarks performing within the same ranges (mostly between $\sim -50\%$ and $\sim 50\%$) regarding gate and depth overhead. In this case, it would be preferable to use the simpler and faster Stochastic1 method. It is important to note that the majority of circuits in Group 0 are real-algorithm-based circuits, including many instances of Grover’s algorithm [78], Cuccaro adder [76] and RevLib [86] algorithms. On the other hand, most circuits in Group 5 are QUEKO circuits [73]. This analysis provides guidance on which types of circuits work better with specific device/mapper configurations.

The Aspen and Rochester device configurations exhibited patterns very similar to Surface 17 and Bristlecone, respectively, for these particular circuit families. Therefore, they were not showcased in this paper. For the rest of the results, refer to Appendix D.

5.2. From single-core to multi-core architectures

Our analysis continues by examining the correlations between the number of inter-core communications and circuit parameters using three different mapping configurations for all-to-all connected multi-core devices: QUBO, HQA, and rOEE, as introduced in Sec.4 (see Fig. 7). Notably, the importance of circuit parameters differs among the mapping techniques. For instance, the number of qubits and maximal cliques is positively correlated with the performance when using HQA, but not with other techniques. Circuit depth and GDG path length mean exhibit a high correlation score (approximately 0.75) with QUBO, while the scores are only 0.2 and 0.4 for the other two mappers. Edge connectivity is not influential when using rOEE, but it is for the other two mappers. Additionally, we explored two different core topologies with the QUBO mapper: all-to-all and grid. Generally, the parameter correlations between these topologies are similar, though some differences exist. For example, the average degree circuit parameter is significantly more important for grid connectivity due to the less connected device connectivity graph, emphasizing the importance of IG connectivity of the circuit, as expected in Sec. 3. We anticipate a larger difference when also reducing the connectivity within the cores, an experiment we leave for future work.

Fig. 7(b) shows an example of the correlation between parameters: edge connectivity, GDG path length mean, and circuit depth, with the number of inter-core

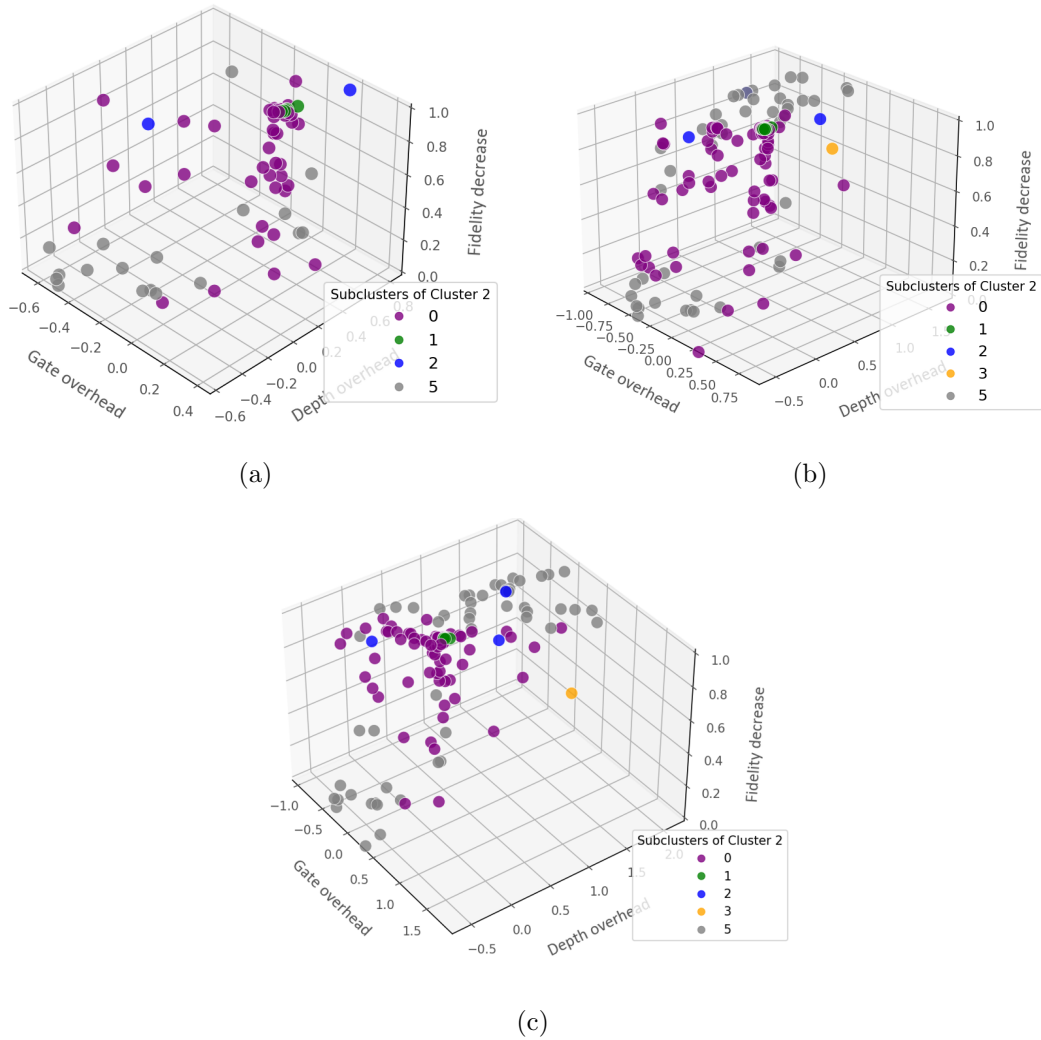


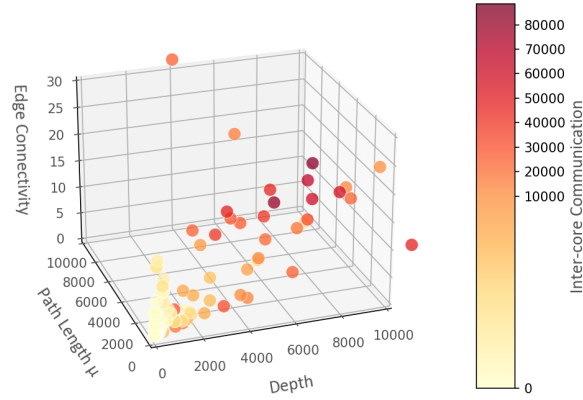
Figure 6: Relation of circuit families (sub-clusters) of cluster 2 with their compilation metrics when targeting: a) Surface 17, b) Bristlecone for Sabre2 mapper, and c) Bristlecone for Stochastic1 mapper.

communications when using the QUBO mapper. A trend is observed where overhead increases with higher metrics values, confirming the high positive correlation shown by their correlation factors in Fig. 7(a).

Similar to single-core devices, we also analyze circuit families and their performance patterns for modular architecture. Fig. 8 shows the groups of circuits that are part of size cluster 0 and their number of moves (inter-core communications) for the two mappers, HQA (a) and rOEE (b). Overall, the HQA mapper performed better, scaling up to 10,000 moves (with only one outlier with 25000) compared to 12,000 for rOEE. rOEE reached that number only for group 4 (pink), making HQA a better choice for this group. Group 0 performed particularly well with both mappers, with all benchmarks having up to 100 moves. Group 4 showcased the worst performance for HQA, reaching up to 10,000 moves, but still significantly better than rOEE. Groups 1 and 5 (blue and

0.77	0.73	0.49	0.42	0.42	0.38	0.35	0.20	0.12	0.08	0.08	0.07	0.05		-0.08	-0.10	-0.12	-0.31	QUBO
0.75	0.75	0.56	0.45	0.48	0.37	0.43	0.21	0.07		0.06	-0.05			-0.09	-0.05	-0.11	-0.30	QUBO Grid
0.22	0.22	0.27	0.45	0.44	0.16	0.41	0.16		0.20		0.25					-0.19	-0.17	HQA
0.20	0.20	0.26	0.52	0.51	0.16	0.48	0.16		0.26	0.05	0.33					-0.21	-0.19	rOEE
Depth	Path Length μ	Critical Paths	Edge Connectivity	Coreness	Clustering Coefficient	Avg. Degree	2-q gate percentage	Idling Score	Qubits	Gates	Max Cliques	Length Of Longest Rep. Subcircuit	% Gates in Critical Path	Longest Repeating Subcircuits	Circuit Density	Pagerank	Central Point Of Dominance	

(a)



(b)

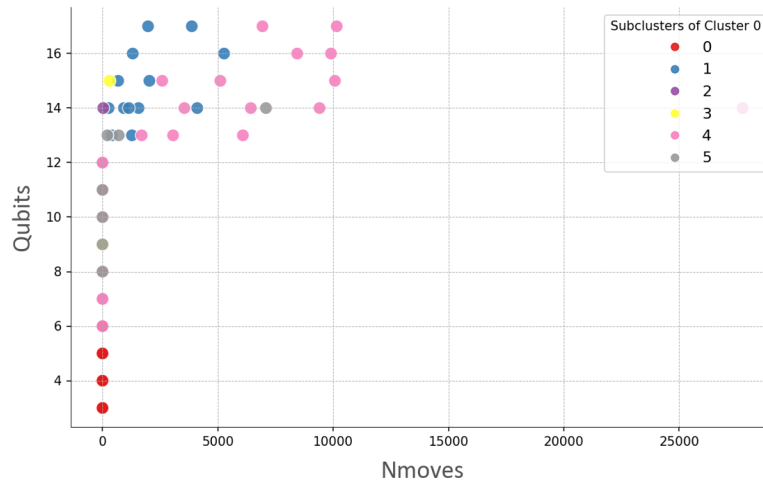
Figure 7: a) Correlation of the number of inter-core communications performance metric with circuit parameters while using 3 different mappers: QUBO, HQA, and rOEE for all-to-all connected cores, and QUBO mapper for grid-like core connectivity. Metrics are ordered from the most positively correlated to the most negatively correlated one. b) Three highly correlated parameters for the QUBO mapper and the all-to-all connected topology: edge connectivity, mean of GDG path length and circuit depth, and their number of inter-core moves.

grey, respectively), on the other hand, showed, on average, a better performance with rOEE, where group 5 outperformed most other groups, despite the higher qubit count. Note that here we do not showcase QUBO results due to lower amount of successfully compiled instances, which would lead to unfair comparison. The results are however available at location shown in Appendix D.

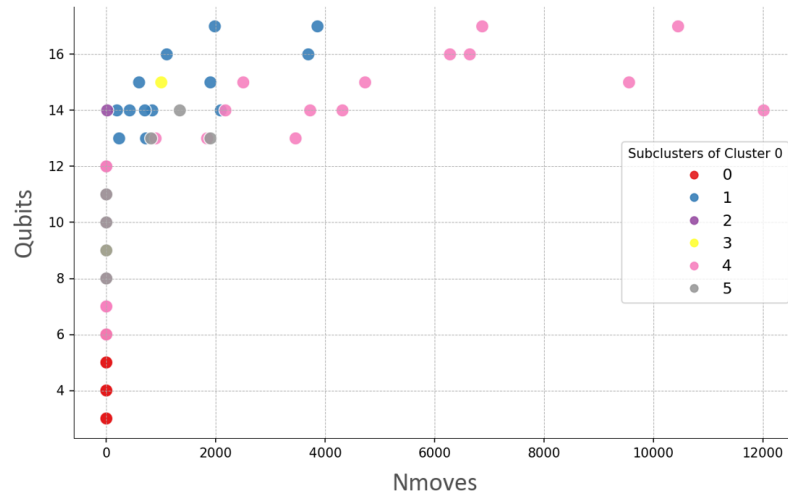
The main insights are as follows:

- There is an evident correlation between the structural parameters of the circuits and their performance, which varies with different compilation and device configurations. This confirms that adapting the quantum system layers to the circuit properties and employing hardware-software co-design is key to successful quantum circuit execution.
- It is possible to make appropriate compilation/device choices per circuit family instead of per single circuit, as there are preferred combinations of device and compilation for each group of similar circuits.

- IG parameters are most important for less connected device topologies.
- Idling and density scores are always of high importance for single-core devices.
- GDG-related parameters and circuit depth are the most relevant metrics for modular architectures, and they are more significant than for single-core architectures.
- Contrary to our expectations, standard parameters like the number of gates, qubits, and the percentage of two-qubit gates, as well as repetitive sub-circuit metrics, are not that significant for circuit success rates.



(a)



(b)

Figure 8: Relation of circuit families (sub-clusters) of cluster 0 with the number of inter-core communications when using all-to-all core connectivity and a) HQA mapper and b) rOEE mapper.

5.3. Evaluating clusters based on circuit origin

The final part of this section showcases the types of clusters created based on the origin of the circuits. We aim to validate that circuits within the same families exhibit similarities not only in their extracted structural parameters but also in their origin. For instance, it stands to reason that randomly generated circuits would share similar structural parameters. This validation would also support the comprehensiveness of the parameter set we used to describe the circuits.

For this purpose, we labeled three groups: real algorithms (based on actual quantum algorithms like Grover’s or arithmetic circuits), randomly generated circuits, and QUEKO circuits (synthetic circuits with predefined depth and gate count) [73]. The circuits were sourced from [22]. Fig. 9 shows the distribution of the existing sub-circuits after a two-level clustering for the modular-architecture-related metrics. We observe that circuits with the same origin generally belong to the same group, with a few outliers. The exceptions are a very small percentage of mixed benchmarks (noted in light brown) and sub-clusters containing both QUEKO and real benchmarks (in mint-green). Since QUEKO circuits aim to mimic realistic behavior more closely than classical random circuits [73], the existence of these mixed groups is expected. The mixed benchmarks group comprises those circuits that are structurally unique compared to other circuits of the same type. This figure confirms that our defined circuit parameters effectively identify structural similarities between circuits, especially highlighting the distinction of randomly generated circuits (green) compared to the other two types that contain logical patterns and oracles.

The complete set of results (for all benchmarks, clusters, compilers and devices) can be found at <https://github.com/QML-Group/QuantumCircuitProfiling>.

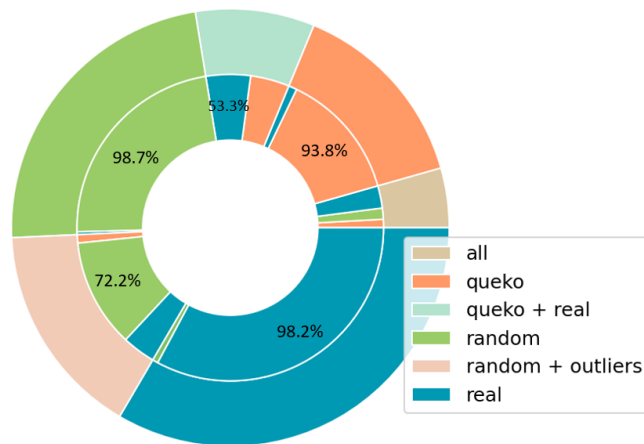


Figure 9: The distribution of the extracted circuit families based on multi-core-architectures circuit parameters per circuit type: Each segment in the outer circle represents groups characterized by the same types of circuits (e.g., the blue segment encompasses circuits based on real algorithms). The inner circle displays the quantity of each circuit type within the respective outer circle segment.

6. Conclusion

To advance the development of future quantum computers and increase the probability of successfully executing algorithms that are currently unfeasible on classical computers, it is crucial to understand their structure. Quantum circuits (i.e., executable versions of quantum algorithms) will yield the highest success rates when run on a quantum system tailored for it. In classical computing, we see two trends that could also shape the future of quantum computers: a) application-specific devices optimized for particular tasks, and b) multi-core computation as a solution for current scalability problems.

In this paper, we explored these aspects within the quantum computing field by introducing the most comprehensive characterization of quantum circuit structures to date. This characterization addresses all facets of quantum circuits: circuit size, qubit interactions, gate density and dependencies, and repetitive patterns. For this purpose, we defined 15 and 19 circuit features of importance for single-core and multi-core quantum devices, respectively. We made special emphasis on modular (i.e., multi-core) architectures, which represent the future of quantum computing and a solution to the scalability challenge of current NISQ devices. Multi-core architecture and related compilation techniques function differently than current quantum systems, because the focus is primarily on reducing the expensive communication between cores. Consequently, extra circuit parameters should be considered for multi-core architectures.

The extracted parameters were used to create families of similarly structured circuits by utilizing the k-means clustering technique. Identifying circuit families simplifies the development of high-performance architectures (by optimizing for families instead of individual circuits), helps to create a representative set of circuits (using cluster representatives), and aids in approximating the performance of future circuits without running them. We also analyzed the types of circuits within the clusters and found that similarly created circuits (real-algorithms, QUEKO, uniformly random) are mostly grouped together. This confirms that our characterization can comprehensively describe a circuit and identify structural similarities between different ones.

Furthermore, we conducted experiments with six different devices and seven mapping configurations to showcase varying correlation levels and performance patterns in terms of gate overhead, depth overhead, fidelity decrease, and number of inter-core communications metrics. These experiments revealed which parameters influence circuit success rates the most, and how these correlations change with different devices or compilers. We could also see that some mappers scale better with the same circuit families than others (e.g., HQA vs. rOEE mapper). Therefore, the patterns observed in clustered circuits can help identify the best existing mapper and device to use, particularly for higher numbers of qubits.

The proposed method and current findings can aid in the development of quantum systems by incorporating information about circuit structure and providing deeper insights into the variability of outcomes when executing different quantum circuits. Structural parameters of circuits can also be used to predict fidelity decrease, gate

overhead, and depth overhead for specific processors and compilation techniques without executing them on actual devices. This can facilitate the co-design of quantum compilers, processors, and applications, ultimately contributing to the development of high-performance application-specific quantum systems. An in-depth analysis of quantum circuits used for benchmarking quantum computing systems is a systematic approach that directly contributes to assessing current devices and lays the foundation for designing future scalable architectures.

7. Acknowledgements

SF and MB acknowledge funding of Intel Corporation. CGA acknowledges funding from the Spanish Ministry of Science, Innovation and Universities through the Beatriz Galindo program 2020 (BG20-00023) and from project PCI2022-133004 funded by MCIN/AEI/10.13039/501100011033 and by the European Union NextGenerationEU/PRTR. CGA, EA and SA also acknowledge support from the EU, grant HORIZON-EIC-2022-PATHFINDEROPEN-01-101099697. Finally, SA acknowledges support from the EU, grant ERC-StG-2021-WINC-101042080.

8. References

- [1] John Preskill. Quantum computing in the nisq era and beyond. *Quantum*, 2:79, 2018.
- [2] Santiago Rodrigo, S. Abadal, Eduard Alarcón, Medina Bandic, Hans van Someren, and Carmen Garcia Almudever. On double full-stack communication-enabled architectures for multicore quantum computers. *IEEE Micro*, 41:48–56, 2021.
- [3] Anabel Ovide, Santiago Rodrigo, Medina Bandic, Hans Van Someren, Sebastian Feld, Sergi Abadal, Eduard Alarcon, and Carmen G Almudever. Mapping quantum algorithms to multicore quantum computing architectures. *Proceedings of the ISCAS '23*, 2023.
- [4] Mohan Sarovar, Timothy Proctor, Kenneth Rudinger, Kevin Young, Erik Nielsen, and Robin Blume-Kohout. Detecting crosstalk errors in quantum information processors. *Quantum*, 4:321, 2020.
- [5] Sergey Bravyi, Oliver Dial, Jay M Gambetta, Darío Gil, and Zaira Nazario. The future of quantum computing with superconducting qubits. *Journal of Applied Physics*, 132(16), 2022.
- [6] James Ang, Gabriella Carini, Yanzhu Chen, Isaac Chuang, Michael Austin DeMarco, Sophia E Economou, Alec Eickbusch, Andrei Faraon, Kai-Mei Fu, Steven M Girvin, et al. Architectures for multinode superconducting quantum computers.(2022). *arXiv preprint arXiv:2212.06167*, 2022.
- [7] C. Monroe, R. Raussendorf, A. Ruthven, K. R. Brown, P. Maunz, L.-M. Duan, and J. Kim. Large-scale modular quantum-computer architecture with atomic memory and photonic interconnects. *Physical Review A*, 89(2), feb 2014.
- [8] Nicholas LaRacuente, Kaitlin N. Smith, Poolad Imany, Kevin L. Silverman, and Frederic T. Chong. Modeling short-range microwave networks to scale superconducting quantum computation. *Preprint at arXiv <https://arxiv.org/abs/2201.08825> v2*, 2023.
- [9] Hamza Jnane, Brennan Undseth, Zhenyu Cai, Simon C Benjamin, and Bálint Koczor. Multicore quantum computing. *arXiv preprint arXiv:2201.08861*, 2022.
- [10] Kaitlin N. Smith, Gokul Subramanian Ravi, Jonathan M. Baker, and Frederic T. Chong. Scaling superconducting quantum computers with chiplet architectures, 2022.
- [11] Medina Bandic, Hossein Zarein, Eduard Alarcon, and Carmen G Almudever. On structured design

- space exploration for mapping of quantum algorithms. In *2020 XXXV Conference on Design of Circuits and Integrated Systems (DCIS)*, pages 1–6. IEEE, 2020.
- [12] Jonathan M Baker, Casey Duckering, Alexander Hoover, and Frederic T Chong. Time-sliced quantum circuit partitioning for modular architectures. In *Proceedings of the 17th ACM International Conference on Computing Frontiers*, pages 98–107, 2020.
 - [13] Medina Bandic, Sebastian Feld, and Carmen G Almudever. Full-stack quantum computing systems in the nisq era: algorithm-driven and hardware-aware compilation techniques. In *2022 Design, Automation & Test in Europe Conference & Exhibition (DATE)*, pages 1–6. IEEE, 2022.
 - [14] Lingling Lao and Dan E. Browne. 2qan: A quantum compiler for 2-local qubit hamiltonian simulation algorithms, 2021.
 - [15] Thomas Lubinski, Sonika Johri, Paul Varosy, Jeremiah Coleman, Luning Zhao, Jason Necaie, Charles H Baldwin, Karl Mayer, and Timothy Proctor. Application-oriented performance benchmarks for quantum computing. *arXiv preprint arXiv:2110.03137*, 2021.
 - [16] Daniel Mills, Seyon Sivarajah, Travis L Scholten, and Ross Duncan. Application-motivated, holistic benchmarking of a full quantum computing stack. *arXiv preprint arXiv:2006.01273*, 2020.
 - [17] Gushu Li, Yufei Ding, and Yuan Xie. Towards efficient superconducting quantum processor architecture design. In *Proceedings of the Twenty-Fifth International Conference on Architectural Support for Programming Languages and Operating Systems*, pages 1031–1045, 2020.
 - [18] Medina Bandic, Carmen G Almudever, and Sebastian Feld. Interaction graph-based characterization of quantum benchmarks for improving quantum circuit mapping techniques. *Quantum Machine Intelligence*, 5(2):40, 2023.
 - [19] Nils Quetschlich, Lukas Burgholzer, and Robert Wille. Predicting good quantum circuit compilation options. In *2023 IEEE International Conference on Quantum Software (QSW)*, pages 43–53. IEEE, 2023.
 - [20] Gushu Li, Yunong Shi, and Ali Javadi-Abhari. Software-hardware co-optimization for computational chemistry on superconducting quantum processors. *arXiv preprint arXiv:2105.07127*, 2021.
 - [21] Lingling Lao and Dan Browne. 2qan: A quantum compiler for 2-local qubit hamiltonian simulation algorithms. *arXiv preprint arXiv:2108.02099*, 2021.
 - [22] Medina Bandic and Nikiforos Paraskevopoulos. qbench benchmark suite. <https://github.com/QML-Group/qbench>, 2021.
 - [23] Nils Quetschlich, Lukas Burgholzer, and Robert Wille. Mqt bench: Benchmarking software and design automation tools for quantum computing. *Quantum*, 7:1062, 2023. MQTbench is available at <https://www.cda.cit.tum.de/mqtbench/>.
 - [24] Teague Tomesh, Pranav Gokhale, Victory Omole, Gokul Subramanian Ravi, Kaitlin N Smith, Joshua Vizslai, Xin-Chuan Wu, Nikos Hardavellas, Margaret R Martonosi, and Frederic T Chong. Supermarq: A scalable quantum benchmark suite. In *2022 IEEE International Symposium on High-Performance Computer Architecture (HPCA)*, pages 587–603. IEEE, 2022.
 - [25] David Freedman, Robert Pisani, and Roger Purves. Statistics (international student edition). *Pisani, R. Purves, 4th edn. WW Norton & Company, New York*, 2007.
 - [26] Santiago Rodrigo, Sergi Abadal, Eduard Alarcón, and Carmen G. Almudever. Will quantum computers scale without inter-chip comms? a structured design exploration to the monolithic vs distributed architectures quest. In *2020 XXXV Conference on Design of Circuits and Integrated Systems (DCIS)*, pages 1–6, 2020.
 - [27] Sergey Bravyi, Oliver Dial, Jay M. Gambetta, Darío Gil, and Zaira Nazario. The future of quantum computing with superconducting qubits. *Journal of Applied Physics*, 132(16), 10 2022.
 - [28] V. Kaushal, B. Lekitsch, A. Stahl, J. Hilder, D. Pijn, C. Schmiegelow, A. Bermudez, M. Müller, F. Schmidt-Kaler, and U. Poschinger. Shuttling-based trapped-ion quantum information processing. *AVS Quantum Science*, 2(1), 03 2020. 014101.

- [29] Brian Marinelli, Jie Luo, Hengjiang Ren, Bethany M. Niedzielski, David K. Kim, Rabindra Das, Mollie Schwartz, David I. Santiago, and Irfan Siddiqi. Dynamically Reconfigurable Photon Exchange in a Superconducting Quantum Processor. 3 2023.
- [30] Carmen G Almudever, Lingling Lao, Robert Wille, and Gian G Guerreschi. Realizing quantum algorithms on real quantum computing devices. In *2020 Design, Automation & Test in Europe Conference & Exhibition (DATE)*, pages 864–872. IEEE, 2020.
- [31] Alwin Zulehner, Alexandru Paler, and Robert Wille. An efficient methodology for mapping quantum circuits to the IBM QX architectures. *IEEE Transactions on Computer-Aided Design of Integrated Circuits and Systems*, 2018.
- [32] Gushu Li, Yufei Ding, and Yuan Xie. Tackling the qubit mapping problem for NISQ-era quantum devices. In *International Conference on Architectural Support for Programming Languages and Operating Systems*, pages 1001–1014, 2019.
- [33] Lingling Lao, Hans van Someren, Imran Ashraf, and Carmen G Almudever. Timing and resource-aware mapping of quantum circuits to superconducting processors. *IEEE Transactions on Computer-Aided Design of Integrated Circuits and Systems*, 2021.
- [34] Toshinari Itoko, Rudy Raymond, Takashi Imamichi, and Atsushi Matsuo. Optimization of quantum circuit mapping using gate transformation and commutation. *Integration*, 70:43–50, 2020.
- [35] Matteo G Pozzi, Steven J Herbert, Akash Sengupta, and Robert D Mullins. Using reinforcement learning to perform qubit routing in quantum compilers. *arXiv preprint arXiv:2007.15957*, 2020.
- [36] Hui Jiang, Yuxin Deng, and Ming Xu. Quantum circuit transformation based on subgraph isomorphism and tabu search. *arXiv preprint arXiv:2104.05214*, 2021.
- [37] Matthew A. Steinberg, Sebastian Feld, Carmen G. Almudever, Michael Marthaler, and Jan-Michael Reiner. Topological-graph dependencies and scaling properties of a heuristic qubit-assignment algorithm. *IEEE Transactions on Quantum Engineering*, 3:1–14, 2022.
- [38] Friedrich Wagner, Andreas Bärmann, Frauke Liers, and Markus Weissenböck. Improving quantum computation by optimized qubit routing. *Journal of Optimization Theory and Applications*, pages 1–34, 2023.
- [39] Prakash Murali, Jonathan M Baker, Ali Javadi-Abhari, Frederic T Chong, and Margaret Martonosi. Noise-adaptive compiler mappings for noisy intermediate-scale quantum computers. In *International Conference on Architectural Support for Programming Languages and Operating Systems*, pages 1015–1029, 2019.
- [40] Swamit S. Tannu and Moinuddin K. Qureshi. Not all qubits are created equal: A case for variability-aware policies for NISQ-era quantum computers. In *International Conference on Architectural Support for Programming Languages and Operating Systems*, pages 987–999, 2019.
- [41] Davide Venturelli, Minh Do, Bryan O’Gorman, Jeremy Frank, Eleanor Rieffel, Kyle EC Booth, Thanh Nguyen, Parvathi Narayan, and Sasha Nanda. Quantum circuit compilation: An emerging application for automated reasoning. 2019.
- [42] Lingling Lao, Bert van Wee, Imran Ashraf, Hans van Someren, Nader Khammassi, Koen Bertels, and Carmen G. Almudever. Mapping of lattice surgery-based quantum circuits on surface code architectures. *Quantum Science and Technology*, 4:015005, 2019.
- [43] Lingling Lao, Daniel M Manzano, Hans van Someren, Imran Ashraf, and Carmen G Almudever. Mapping of quantum circuits onto nistq superconducting processors. *arXiv preprint arXiv:1908.04226*, 2019.
- [44] Steven Herbert and Akash Sengupta. Using reinforcement learning to find efficient qubit routing policies for deployment in near-term quantum computers. *arXiv:1812.11619*, 2018.
- [45] Aaron Lye, Robert Wille, and Rolf Drechsler. Determining the minimal number of swap gates for multi-dimensional nearest neighbor quantum circuits. In *Asia and South Pacific Design Automation Conference*, pages 178–183, 2015.
- [46] Sanjiang Li, Xiangzhen Zhou, and Yuan Feng. Qubit mapping based on subgraph isomorphism and filtered depth-limited search. *IEEE Transactions on Computers*, 2020.

- [47] Amirmohammad Biuki, Naser Mohammadzadeh, Robert Wille, and Sahar Sargaran. Exact mapping of quantum circuit partitions to building blocks of the saqip architecture. In *2022 IEEE Computer Society Annual Symposium on VLSI (ISVLSI)*, pages 402–405. IEEE, 2022.
- [48] Abtin Molavi, Amanda Xu, Martin Diges, Lauren Pick, Swamit Tannu, and Aws Albarghouthi. Qubit mapping and routing via maxsat. In *2022 55th IEEE/ACM International Symposium on Microarchitecture (MICRO)*, pages 1078–1091. IEEE, 2022.
- [49] Lorenzo Moro, Matteo GA Paris, Marcello Restelli, and Enrico Prati. Quantum compiling by deep reinforcement learning. *Communications Physics*, 4(1):178, 2021.
- [50] Dhruv Devulapalli, Eddie Schoute, Aniruddha Bapat, Andrew M. Childs, and Alexey V. Gorshkov. Quantum routing with teleportation, 2022.
- [51] Suryansh Upadhyay, Abdullah Ash Saki, Rasit Onur Topaloglu, and Swaroop Ghosh. A shuttle-efficient qubit mapper for trapped-ion quantum computers. In *Proceedings of the Great Lakes Symposium on VLSI 2022*, pages 305–308, 2022.
- [52] Natalia Nottingham, Michael A Perlin, Ryan White, Hannes Bernien, Frederic T Chong, and Jonathan M Baker. Decomposing and routing quantum circuits under constraints for neutral atom architectures. *arXiv preprint arXiv:2307.14996*, 2023.
- [53] Nikiforos Paraskevopoulos, Fabio Sebastiano, Carmen G Almudever, and Sebastian Feld. Spinq: Compilation strategies for scalable spin-qubit architectures. *arXiv preprint arXiv:2301.13241*, 2023.
- [54] Matthew Steinberg, Medina Bandic, Sacha Szkudlarek, Carmen G Almudever, Aritra Sarkar, and Sebastian Feld. Resource bounds for quantum circuit mapping via quantum circuit complexity. *arXiv preprint arXiv:2402.00478*, 2024.
- [55] Bochen Tan and Jason Cong. Optimal qubit mapping with simultaneous gate absorption. *arXiv preprint arXiv:2109.06445*, 2021.
- [56] Robin Blume-Kohout and Kevin C Young. A volumetric framework for quantum computer benchmarks. *Quantum*, 4:362, 2020.
- [57] Santiago Rodrigo, Medina Bandic, Sergi Abadal, Hans van Someren, Eduard Alarcón, and Carmen G. Almudéver. Scaling of multi-core quantum architectures: A communications-aware structured gap analysis. In *Proceedings of Computing Frontiers '21*, page 144–151, 2021.
- [58] Santiago Rodrigo, Domenico Spanò, Medina Bandic, Sergi Abadal, Hans Van Someren, Anabel Ovide, Sebastian Feld, Carmen G Almudéver, and Eduard Alarcón. Characterizing the spatio-temporal qubit traffic of a quantum intranet aiming at modular quantum computer architectures. In *Proceedings of the 9th ACM International Conference on Nanoscale Computing and Communication*, pages 1–7, 2022.
- [59] Sahar Ben Rached, Isaac Lopez Agudo, Santiago Rodrigo, Medina Bandic, Sebastian Feld, Hans van Someren, Eduard Alarcón, Carmen G Almudéver, and Sergi Abadal. Characterizing the inter-core qubit traffic in large-scale quantum modular architectures. *arXiv preprint arXiv:2310.01921*, 2023.
- [60] Daniele Cuomo, Marcello Caleffi, Kevin Krsulich, Filippo Tramonto, Gabriele Agliardi, Enrico Prati, and Angela Sara Cacciapuoti. Optimized compiler for distributed quantum computing. *ACM Transactions on Quantum Computing*, 4(2), 2023.
- [61] Davide Ferrari, Angela Sara Cacciapuoti, Michele Amoretti, and Marcello Caleffi. Compiler design for distributed quantum computing. *arXiv preprint arXiv:2012.09680*, 2020.
- [62] Medina Bandic, Luise Prielinger, Jonas Nußlein and, Anabel Ovide, Santiago Rodrigo, Sergi Abadal, Hans van Someren, Gayane Vardoyan, Eduard Alarcon, Carmen G. Almudever, and Sebastian Feld. Mapping quantum circuits to modular architectures with qubo. In *2023 IEEE International Conference on Quantum Computing and Engineering (QCE)*, pages 790–801, Los Alamitos, CA, USA, sep 2023. IEEE Computer Society.
- [63] Pau Escofet, Anabel Ovide, Carmen G Almudever, Eduard Alarcón, and Sergi Abadal. Hungarian qubit assignment for optimized mapping of quantum circuits on multi-core architectures. *IEEE Computer Architecture Letters*, 2023.

- [64] Pau Escofet, Anabel Ovide, Medina Bandic, Luise Prielinger, Hans van Someren, Sebastian Feld, Eduard Alarcón, Sergi Abadal, and Carmen G Almudéver. Revisiting the mapping of quantum circuits: Entering the multi-core era. *ACM Transactions on Quantum Computing*, 2024.
- [65] Javier Martín Hernández and Piet Van Mieghem. Classification of graph metrics. *Delft University of Technology: Mekelweg, The Netherlands*, pages 1–20, 2011.
- [66] Sergey Brin and Lawrence Page. The anatomy of a large-scale hypertextual web search engine. *Computer Networks*, 30:107–117, 1998.
- [67] Wikipedia. Longest repeated substring problem. https://en.wikipedia.org/wiki/Longest_repeated_substring_problem, 2024.
- [68] Seth Lloyd. Least squares quantization in pcm. *IEEE Transactions on Information Theory*, 28(2):129–137, 1982.
- [69] Peter J Rousseeuw. Silhouettes: a graphical aid to the interpretation and validation of cluster analysis. *Journal of computational and applied mathematics*, 20:53–65, 1987.
- [70] QUTECH. Quantum inspire, 2020.
- [71] MD Sajid Anis et al. Qiskit: An open-source framework for quantum computing, 2021.
- [72] Nader Khammassi, Imran Ashraf, JV Someren, Razvan Nane, AM Krol, M Adriaan Rol, Lingling Lao, Koen Bertels, and Carmen G Almudéver. Openql: A portable quantum programming framework for quantum accelerators. *ACM Journal on Emerging Technologies in Computing Systems (JETC)*, 18(1):1–24, 2021.
- [73] UCLA. Queko benchmark. <https://github.com/UCLA-VAST/QUEKO-benchmark>, 2020.
- [74] Diogo Valada. Openql random circuits. https://github.com/Astlaan/OpenQL/blob/metrics/tools/random_circuit_generator.py, 2020.
- [75] Andrew W Cross, Lev S Bishop, Sarah Sheldon, Paul D Nation, and Jay M Gambetta. Validating quantum computers using randomized model circuits. *Physical Review A*, 100(3):032328, 2019.
- [76] Steven Cuccaro, Thomas Draper, Samuel Kutin, and David Moulton. A new quantum ripple-carry addition circuit. 11 2004.
- [77] Daniel M. Greenberger, Michael A. Horne, and Anton Zeilinger. Going beyond bell’s theorem, 2007.
- [78] Michael A Nielsen and Isaac Chuang. Quantum computation and quantum information, 2002.
- [79] IBM. <https://www.ibm.com/quantum>.
- [80] Rigetti. <https://medium.com/rigetti/>.
- [81] Timothy D. Goodrich, Eric Horton, and Blair D. Sullivan. Practical graph bipartization with applications in near-term quantum computing. *ArXiv*, abs/1805.01041, 2018.
- [82] Harold W Kuhn. The hungarian method for the assignment problem. *Naval research logistics quarterly*, 2(1-2):83–97, 1955.
- [83] Abraham P Punnen. *The Quadratic Unconstrained Binary Optimization Problem*. Springer, 2022.
- [84] Prakash Murali, Norbert Matthias Linke, Margaret Martonosi, Ali Javadi Abhari, Nhung Hong Nguyen, and Cinthia Huerta Alderete. Full-stack, real-system quantum computer studies: Architectural comparisons and design insights. In *2019 ACM/IEEE 46th Annual International Symposium on Computer Architecture (ISCA)*, pages 527–540. IEEE, 2019.
- [85] Shin Nishio, Yulu Pan, Takahiko Satoh, Hideharu Amano, and Rodney Van Meter. Extracting success from ibm’s 20-qubit machines using error-aware compilation. *ACM Journal on Emerging Technologies in Computing Systems (JETC)*, 16(3):1–25, 2020.
- [86] Robert Wille, Daniel Große, Lisa Teuber, Gerhard W Dueck, and Rolf Drechsler. Revlib: An online resource for reversible functions and reversible circuits. In *38th International Symposium on Multiple Valued Logic (ismvl 2008)*, pages 220–225. IEEE, 2008.

Appendix A. Selected quantum benchmarks

Table A1: Benchmarks used for the experiments.

Benchmark	Qubits	Gates	Two-qubit gate percentage
0410184_169	14	211	0.492890995
15_enc	15	264	0.522727273
16QBT_100CYC_QSE_1	16	1400	0.327142857
16QBT_10CYC_TFL_1	16	1473	0.330617787
16QBT_15CYC_TFL_2	16	1582	0.335651075
16QBT_20CYC_TFL_3	16	1727	0.341053851
16QBT_35CYC_TFL_6	16	1980	0.348484848
16QBT_40CYC_TFL_7	16	2269	0.355222565
16QBT_500CYC_QSE_3	16	7949	0.302679582
16QBT_700CYC_QSE_5	16	15901	0.292182882
16QBT_900CYC_QSE_7	16	26125	0.288076555
20QBT_100CYC_QSE_8	20	27545	0.287747323
20QBT_400CYC_QSE_8	20	33225	0.286711813
20QBT_45CYC_0D1_1D2_0	15	33270	0.287676586
20QBT_45CYC_0D1_1D2_5	13	33315	0.288638751
20QBT_45CYC_0D1_2D2_0	20	33405	0.290555306
20QBT_45CYC_0D1_2D2_5	20	33495	0.292461561
20QBT_45CYC_0D1_2D2_9	20	33585	0.2943576
20QBT_45CYC_0D1_3D2_0	20	33720	0.297182681
20QBT_45CYC_0D1_3D2_5	20	33855	0.299985231
20QBT_45CYC_0D1_3D2_9	20	33990	0.302765519
20QBT_45CYC_0D1_4D2_0	20	34170	0.306438396
20QBT_45CYC_0D1_5D2_1	20	34395	0.310975432
20QBT_45CYC_0D1_6D2_2	20	34665	0.316342132
20QBT_45CYC_0D1_7D2_3	20	34980	0.322498571
20QBT_45CYC_0D1_8D2_4	20	35340	0.329400113
20QBT_45CYC_1D1_1D2_5	20	35475	0.329415081
20QBT_45CYC_1D1_2D2_6	20	35655	0.330276259
20QBT_45CYC_1D1_3D2_7	20	35880	0.33196767
20QBT_45CYC_1D1_4D2_8	20	36150	0.334467497
20QBT_45CYC_1D1_5D2_9	20	36465	0.337748526
20QBT_45CYC_1D1_6D2_0	20	36825	0.341778683
20QBT_45CYC_1D1_7D2_1	20	37230	0.346521622
20QBT_45CYC_2D1_2D2_3	20	37500	0.346426667
20QBT_45CYC_2D1_3D2_4	20	37815	0.347110935
20QBT_45CYC_2D1_4D2_5	20	38175	0.348552718
20QBT_45CYC_2D1_5D2_6	20	38580	0.350725765
20QBT_45CYC_2D1_6D2_7	20	39030	0.353599795
20QBT_45CYC_3D1_1D2_8	17	39345	0.351912568
20QBT_45CYC_3D1_2D2_9	20	39705	0.35098854
20QBT_45CYC_3D1_3D2_0	20	40110	0.350810272
20QBT_45CYC_3D1_4D2_1	20	40560	0.351356016
20QBT_45CYC_3D1_5D2_2	20	41055	0.352600171
20QBT_45CYC_4D1_1D2_3	19	41460	0.350241196
20QBT_45CYC_4D1_2D2_4	20	41910	0.348628012
20QBT_45CYC_4D1_3D2_5	20	42405	0.347742012
20QBT_45CYC_4D1_4D2_6	20	42945	0.347560834
20QBT_45CYC_5D1_1D2_7	20	43440	0.34463628
20QBT_45CYC_5D1_2D2_8	20	43980	0.342451114
20QBT_45CYC_5D1_3D2_9	20	44565	0.340985078
20QBT_45CYC_6D1_2D2_1	20	45195	0.338223255
20QBT_500CYC_QSE_7	20	52295	0.330547854
20QBT_800CYC_QSE_4	20	63655	0.321828607
20QBT_900CYC_QSE_3	20	76435	0.31511742
3_17_13	3	76471	0.31519138
4gt10-v1_81	5	76619	0.31544395
4gt11_82	5	76646	0.315567675
4gt12-v0_87	6	76893	0.31601056
4gt13_92	5	76959	0.316129368
4gt4-v0_72	6	77217	0.316536514
4gt5_75	5	77300	0.316688228
4mod5-bdd_287	7	77370	0.316802378
4mod7-v0_94	5	77532	0.317069081
4_49_16	5	77749	0.317457459
53QBT_700CYC_QSE_3	53	104091	0.308412831
54QBT_10CYC_QSE_9	54	104475	0.308312994
54QBT_15CYC_QSE_8	54	105051	0.308164606
54QBT_200CYC_QSE_7	54	112719	0.306363612
54QBT_25CYC_QSE_6	54	113678	0.306154225
54QBT_35CYC_QSE_4	54	115020	0.305868545
54QBT_40CYC_QSE_3	54	116554	0.305549359
54QBT_500CYC_QSE_0	54	135724	0.302179423
54QBT_800CYC_QSE_7	54	166396	0.298402606
9symml_195	11	201277	0.322366689
adder_n10	10	201571	0.32221897
adder_n4	4	201594	0.322231812
adr4_197	13	205033	0.324133188
aj-e11_165	5	205184	0.324230934
alu-bdd_288	7	205268	0.324283376
alu-v0_26	5	205352	0.324335775
alu-v1_28	5	205389	0.324364985
alu-v2_30	6	205893	0.324654068
alu-v2_31	5	206344	0.324904044
alu-v3_34	5	206396	0.324938468
alu-v4_36	5	206511	0.325004479
basis_change_n3	3	206590	0.324928603

Continued on next page

Table A1 – continued from previous page

Benchmark	Qubits	Gates	Two-qubit gate percentage
basis_trotter_n4	4	208528	0.323836607
bell_n4	4	208577	0.32379409
benstein_vazirani_1b_secret_1	2	208584	0.323792812
benstein_vazirani_28b_secret_64	2	208645	0.323707733
bigadder_n18	18	209231	0.323422437
bv_n14	14	209272	0.323421193
bv_n19	19	209328	0.32342066
C17_204	7	209795	0.323677876
cat_state_n4	4	209799	0.323686004
cm82a_208	8	210449	0.324031
cnt3-5_179	16	210624	0.324165337
col4_215	15	228560	0.333028526
con1_216	9	229514	0.333452426
cuccaroAdder_10b	22	230235	0.333107477
CuccaroAdder_1b	4	230308	0.333075707
cuccaroadder_q128	127	232979	0.333785448
cuccaroadder_q16	15	233258	0.333827779
cuccaroadder_q32	31	233897	0.333937588
cuccaroadder_q64	63	235256	0.334180637
cuccaroMultiplier_1b	5	235432	0.334066737
cycle10_2_110	12	241482	0.336662774
dc1_220	11	243396	0.337437756
dc2_222	15	252858	0.341147996
decod24-v1_41	5	252943	0.341183587
deutsch_n2	2	252948	0.341180796
dist_223	13	290994	0.353701451
dnn_n16	16	294034	0.351350524
dnn_n2	2	294372	0.351089778
dnn_n8	8	295892	0.349935111
error_correctiond3_n5	5	296005	0.349967061
ex-1_166	3	296024	0.349975002
ex3_229	6	296427	0.350089567
f2_232	8	297633	0.350434932
fredkin_n3	3	297652	0.350439439
ghz_q128	127	297779	0.350713113
ghz_q16	15	297810	0.350723616
ghz_q32	31	297841	0.350787836
ghz_q64	64	297905	0.350923952
graycode6_47	6	297910	0.350934846
grover_n2	2	297926	0.350922712
grover_n3	3	298015	0.350858178
grover_operator_8	8	298506	0.351554073
grover_q128_1	127	303497	0.350675624
grover_q16_1	15	304008	0.350559854
grover_q32_1	31	305159	0.350338676
grover_q64	63	307590	0.349910595
ham7_104	7	307910	0.350030853
hwb7_59	8	332289	0.356493895
inc_237	16	342908	0.358973836
ising_model_13	13	343541	0.358661703
iswap_n2	2	343550	0.358658128
life_238	11	365995	0.363439391
linearsolver_n3	3	366018	0.363427482
lpn_n5	3	366029	0.363422024
majority_239	7	366641	0.36354363
max46_240	10	393767	0.368578372
miller_11	3	393817	0.36858998
mini-alu_167	5	394105	0.368640337
misex1_241	15	398918	0.369456881
mlp4_245	16	417770	0.372489647
mod10_171	5	418014	0.372530585
mod5adder_127	6	418569	0.372607623
mod5d2_64	5	418622	0.372620168
multiplier_n15	15	419880	0.372089645
multiply_n13	11	420020	0.372027522
one-two-three-v1_99	5	420152	0.372051067
plus63mod4096_163	13	548896	0.387408544
pml_249	14	550672	0.3875592
q=10_s=19990_2qbf=02_1	10	570672	0.380798427
q=10_s=19990_2qbf=05_1	10	590672	0.384963228
q=10_s=2990_2qbf=03_1	10	593672	0.384581048
q=10_s=29990_2qbf=05_1	10	623672	0.390166626
q=10_s=39990_2qbf=08_1	10	663672	0.414793754
q=10_s=49990_2qbf=09_1	10	713672	0.448717338
q=10_s=50_2qbf=096_1	10	713732	0.448746869
q=10_s=90_2qbf=011_1	9	713832	0.448698013
q=10_s=990_2qbf=091_1	10	714832	0.449327954
q=11_s=19989_2qbf=01_1	11	734832	0.439857001
q=11_s=2989_2qbf=02_1	11	737832	0.438870908
q=11_s=29989_2qbf=03_1	11	767832	0.433373446
q=11_s=39989_2qbf=05_1	11	807832	0.436708375
q=11_s=49989_2qbf=08_1	11	857832	0.458122336
q=11_s=49_2qbf=061_1	11	857892	0.458126431
q=11_s=89_2qbf=022_1	10	857992	0.458092849
q=11_s=989_2qbf=081_1	11	858992	0.458500196
q=12_s=19988_2qbf=01_1	12	878992	0.450404554
q=12_s=29988_2qbf=03_1	12	908992	0.445463766

Continued on next page

Table A1 – continued from previous page

Benchmark	Qubits	Gates	Two-qubit gate percentage
q=12.s=49988.2qbf=05.1	12	958992	0.448407286
q=12.s=59988.2qbf=09.1	12	1018992	0.475073406
q=12.s=9988.2qbf=01.1	12	1028992	0.471399195
q=13.s=19987.2qbf=01.1	13	1048992	0.464347679
q=13.s=29987.2qbf=02.1	13	1078992	0.457022851
q=13.s=49987.2qbf=03.1	13	1128992	0.449958901
q=13.s=59987.2qbf=05.1	13	1188992	0.452428612
q=13.s=9987.2qbf=08.1	13	1198992	0.455379185
q=14.s=19986.2qbf=09.1	14	1218992	0.462717557
q=14.s=29986.2qbf=01.1	14	1248992	0.454013316
q=14.s=39986.2qbf=02.1	14	1288992	0.44615017
q=14.s=49986.2qbf=03.1	14	1338992	0.440653118
q=14.s=5986.2qbf=03.1	14	1344992	0.440031614
q=14.s=5986.2qbf=05.1	14	1350992	0.440291282
q=14.s=59986.2qbf=08.1	14	1410992	0.455618459
q=14.s=986.2qbf=051.1	14	1411992	0.455654848
q=14.s=9986.2qbf=09.1	14	1421992	0.458755745
q=15.s=19985.2qbf=01.1	15	1441992	0.453747316
q=15.s=29985.2qbf=02.1	15	1471992	0.448508552
q=15.s=49985.2qbf=03.1	15	1521992	0.443598258
q=15.s=59985.2qbf=05.1	15	1581992	0.445789865
q=15.s=985.2qbf=051.1	15	1582992	0.445810213
q=15.s=9985.2qbf=08.1	15	1592992	0.448015433
q=16.s=19984.2qbf=09.1	16	1612992	0.453625312
q=16.s=29984.2qbf=01.1	16	1642992	0.447171738
q=16.s=49984.2qbf=02.1	16	1692992	0.439795345
q=16.s=59984.2qbf=03.1	16	1752992	0.434988865
q=16.s=984.2qbf=051.1	16	1753992	0.435031061
q=17.s=19983.2qbf=05.1	17	1773992	0.435784942
q=17.s=2983.2qbf=08.1	17	1776992	0.436393636
q=17.s=29983.2qbf=09.1	17	1806992	0.444058413
q=17.s=43.2qbf=028.1	12	1807052	0.44405031
q=17.s=49983.2qbf=01.1	17	1857052	0.434774578
q=17.s=5983.2qbf=02.1	17	1863052	0.434022239
q=17.s=59983.2qbf=03.1	17	1923052	0.42978349
q=17.s=983.2qbf=031.1	17	1924052	0.42970928
q=17.s=9983.2qbf=05.1	17	1934052	0.430105292
q=3.s=19997.2qbf=01.1	3	1954052	0.426738388
q=3.s=2997.2qbf=01.1	3	1957052	0.42625592
q=3.s=2997.2qbf=02.1	3	1960052	0.425914721
q=3.s=29997.2qbf=03.1	3	1990052	0.423986408
q=3.s=39997.2qbf=05.1	3	2030052	0.42552309
q=3.s=57.2qbf=011.1	3	2030112	0.425511991
q=3.s=5997.2qbf=08.1	3	2036112	0.426616021
q=3.s=59997.2qbf=09.1	3	2096112	0.440210256
q=3.s=97.2qbf=01.1	3	2096212	0.440194026
q=3.s=997.2qbf=02.1	3	2097212	0.440084264
q=3.s=9997.2qbf=03.1	3	2107212	0.439416632
q=4.s=19996.2qbf=02.1	4	2127212	0.437199959
q=4.s=19996.2qbf=05.1	4	2147212	0.437750441
q=4.s=2996.2qbf=08.1	4	2150212	0.438275389
q=4.s=29996.2qbf=09.1	4	2180212	0.444609056
q=4.s=39996.2qbf=01.1	4	2220212	0.438430654
q=4.s=49996.2qbf=02.1	4	2270212	0.433220774
q=4.s=49996.2qbf=09.1	4	2320212	0.443277166
q=4.s=56.2qbf=032.1	4	2320272	0.44327303
q=4.s=96.2qbf=052.1	4	2320372	0.443277199
q=4.s=996.2qbf=03.1	4	2321372	0.443202985
q=4.s=9996.2qbf=05.1	4	2331376	0.443385794
q=5.s=19995.2qbf=03.1	5	2351376	0.442204479
q=5.s=19995.2qbf=08.1	5	2371376	0.445262582
q=5.s=2995.2qbf=09.1	5	2374376	0.445835874
q=5.s=39995.2qbf=01.1	5	2414376	0.440142298
q=5.s=49995.2qbf=02.1	5	2464376	0.435259473
q=5.s=55.2qbf=087.1	5	2464436	0.435269571
q=5.s=95.2qbf=095.1	5	2464536	0.435288428
q=5.s=9995.2qbf=03.1	5	2474536	0.434721903
q=6.s=19994.2qbf=05.1	6	2494536	0.435235651
q=6.s=2994.2qbf=08.1	6	2497536	0.435676202
q=6.s=29994.2qbf=09.1	6	2527536	0.441167604
q=6.s=49994.2qbf=01.1	6	2577536	0.434544852
q=6.s=54.2qbf=022.1	6	2577596	0.434540168
q=6.s=94.2qbf=053.1	6	2577696	0.434543484
q=6.s=9994.2qbf=02.1	6	2587696	0.433640196
q=7.s=19993.2qbf=03.1	7	2607696	0.432629417
q=7.s=2993.2qbf=05.1	7	2610696	0.432714495
q=7.s=2993.2qbf=08.1	7	2613696	0.433130708
q=7.s=29993.2qbf=08.1	7	2643696	0.437292336
q=7.s=39993.2qbf=09.1	7	2683696	0.444200088
q=7.s=53.2qbf=034.1	7	2683756	0.44419761
q=7.s=59993.2qbf=09.1	7	2743756	0.454141695
q=7.s=93.2qbf=054.1	7	2743856	0.454144095
q=7.s=993.2qbf=081.1	7	2744856	0.454264996
q=8.s=19992.2qbf=02.1	8	2764856	0.452427902
q=8.s=2992.2qbf=01.1	8	2767856	0.452036883
q=8.s=2992.2qbf=03.1	8	2770856	0.451846289
q=8.s=29992.2qbf=05.1	8	2800856	0.452341356

Continued on next page

Table A1 – continued from previous page

Benchmark	Qubits	Gates	Two-qubit gate percentage
q=8.s=39992.2qbf=08.1	8	2840856	0.457238593
q=8.s=49992.2qbf=09.1	8	2890856	0.464903129
q=8.s=52.2qbf=104.1	8	2890916	0.464911468
q=8.s=92.2qbf=011.1	8	2891016	0.464901267
q=8.s=992.2qbf=081.1	8	2892016	0.465010567
q=9.s=19991.2qbf=08.1	9	2912016	0.467286924
q=9.s=2991.2qbf=01.1	9	2915016	0.466909959
q=9.s=51.2qbf=012.1	7	2915076	0.46690275
q=9.s=51.2qbf=059.1	9	2915136	0.466902745
q=9.s=91.2qbf=088.1	9	2915236	0.466914514
q=9.s=991.2qbf=091.1	9	2916236	0.467064394
qaoa.WS.128	128	2917388	0.467055462
qaoa.WS.16	16	2917532	0.467054346
qaoa.WS.32	32	2917820	0.467052114
qaoa.WS.64	64	2918396	0.467047652
qaoa.128	128	2931068	0.467823333
qaoa.16	15	2931579	0.467790907
qaoa.32	31	2932730	0.467721884
qaoa.64	64	2935937	0.467895599
qaoa.n6	6	2936351	0.46784802
qec.en.n5	5	2936376	0.467847442
qec.sm.n5	5	2936401	0.467846864
qft.8	8	2936577	0.467841981
qft.n15	15	2937117	0.467827465
qft.n20	20	2938087	0.467802349
qft.q128	128	2970919	0.468104314
qft.q16	16	2971439	0.468103165
qft.q32	32	2973503	0.468111853
qft.q64	64	2981727	0.468172975
QuantumVolume.128	128	3178463	0.454658745
QuantumVolume.16	16	3181551	0.454458847
QuantumVolume.32	32	3193871	0.453667665
QuantumVolume.64	64	3243087	0.45057194
quantum.volume.8	8	3243951	0.450481527
quantum.volume.n5	5	3244289	0.450445691
queko.128	128	3252482	0.450318557
queko.16	16	3252611	0.450316684
queko.32	32	3253124	0.450308688
queko.64	64	3255173	0.450277143
queko.8	8	3255205	0.450276403
radd.250	13	3258418	0.450263594
rd32.270	5	3258502	0.450263035
rd53.311	13	3258777	0.450263089
rd73.140	10	3259007	0.450263224
rd73.252	10	3264328	0.450239682
rd84.142	15	3264671	0.450239549
root.255	13	3281830	0.450168656
sao2.257	14	3320407	0.450017423
sat.n11	11	3321884	0.449893193
seca.n11	11	3322217	0.449873383
sf.274	6	3322998	0.449868763
shor.15	11	3327790	0.449758248
shor.35	15	3344319	0.449359944
simon.n6	5	3344401	0.449353113
sqn.258	10	3354624	0.449312948
sqrt8.260	12	3357633	0.449301636
squar5.261	13	3359626	0.449293761
square.root.7	15	3367256	0.449193052
sym9.148	10	3388760	0.449118852
sys6-v0.111	10	3388975	0.449119276
teleportation.n3	3	3388983	0.449118806
toffoli.n3	3	3389001	0.449118191
urf5.280	9	3438830	0.449520913
variational.n4	4	3438884	0.449518507
vbeAdder.1b	4	3438954	0.449513428
vbeAdder.5b	16	3439584	0.449467726
VQEHEA1.128	128	3443414	0.449336618
VQEHEA1.16	16	3443884	0.44931885
VQEHEA1.32	32	3444834	0.449284929
VQEHEA1.64	64	3446744	0.449218741
VQEHEA2.128	128	3450574	0.449088181
VQEHEA2.16	16	3451044	0.449070484
VQEHEA2.32	32	3451994	0.449036702
VQEHEA2.64	64	3453904	0.448970788
vqe.uccsd.n4	4	3454124	0.448967669
vqe.uccsd.n6	6	3456406	0.448975612
vqe.uccsd.n8	8	3467214	0.449158892
wim.266	11	3468200	0.449154316
wstate.n3	3	3468249	0.449150566
xor5.254	6	3468256	0.449151101
z4.268	11	3471329	0.449140372

Appendix B. Generating GDG parameters

The construction of the GDG is done by a linear scan of the circuit, adding a new node w for each gate. For each newly added gate node operating on n qubits $(q_i)_{i=1}^n$, the algorithm adds incoming edges $(v_1, w), \dots, (v_n, w)$ such that v_i is the last gate operating on qubit q_i . This last information is stored in and retrieved from an array that maps qubit indices to the last gate using said qubit. When no such gate exists, the edge comes from an extra sentinel node called **source**. After all gates are processed, all children-less nodes are linked to another sentinel node called the **sink**.

Since a quantum gate cannot depend on itself, the resulting directed graph is always *acyclic*, therefore constitutes a *directed acyclic graph* (DAG). We ignore the trivial case where this DAG is not weakly connected. Any *topological ordering* of the nodes gives a valid sequential order for the gates during circuit execution.

The *critical path length* is easily computed with an existing library, for instance using `networkx.dag_longest_path_length`. Our other metrics require however custom processing of the graph, since brute-force extraction is doomed to fail for large circuits: for instance, in some DAG families, the *number of critical paths* grows exponentially with the number of circuit gates.

Our solution is to *recursively* compute those metrics. The recurrence relations between a node’s values and the values of its children are given in Tab. B1. Our Python implementation (see Appendix D) is made iterative instead of recursive using a bottom-up traversal of the GDG, where nodes are iterated in *reversed* topological ordering.

Appendix C. Clustering settings and examples

Table C1: K-Means settings: Single-core architecture

Cluster	n_clusters	Silhouette coef.
size	5	0.473
0	4	0.312
1	6	0.290
2	7	0.319
3	1	-
4	7	0.352

Table C2: K-Means settings: Multi-core architecture

Cluster	n_clusters	Silhouette coef.
size	5	0.473
0	6	0.386
1	6	0.342
2	10	0.349
3	1	-
4	6	0.288

To cluster the benchmarks according to the specified parameters, we utilize K-Means, a centroid-based clustering algorithm [68]. The configuration of this algorithm is detailed in Table C2, where the first column indicates the number of size-based clusters, the second column represents the number of structure-based sub-clusters within each cluster, and the third column showcases their respective Silhouette coefficients, guiding

Metric	Initialisation and recurrence relation
Number of gates in critical paths to sink (L)	$L(\mathbf{sink}) = 0$ $L(w) = 1 + \max_i L(v_i)$ <p>From that we can define an edge predicate describing whether a given edge (w, v_i) belongs to a critical path:</p> $\mathbf{CP}(w, v_i) = \top \text{ if } L(w) = 1 + L(v_i), \perp \text{ otherwise.}$
Number of paths to sink (n)	$n(\mathbf{sink}) = 1$ $n(w) = \sum_i n(v_i)$
Number of critical paths to sink (N)	$N(\mathbf{sink}) = 1$ $N(w) = \sum_{i \mid \mathbf{CP}(w, v_i)} N(v_i)$
Max number of two-qubit gates in critical paths to sink (M)	$M(\mathbf{sink}) = 0$ $M(w) = \begin{cases} 1 + \max_{i \mid \mathbf{CP}(w, v_i)} M(v_i) & \text{if } w \text{ is a 2-qubit gate} \\ \max_{i \mid \mathbf{CP}(w, v_i)} M(v_i) & \text{otherwise} \end{cases}$
Number of critical paths to sink with max two-qubit gates (K)	$K(\mathbf{sink}) = 1$ $K(w) = \sum_{i \mid \mathbf{CP}(w, v_i) \wedge M(v_i) + 1 = M(w)} K(v_i)$
Mean length of paths to sink (m)	$m(\mathbf{sink}) = 0$ $m(w) = \frac{1}{n(w)} \sum_i n(v_i) (m(v_i) + 1)$
Variance of length of paths to sink (v)	$v(\mathbf{sink}) = 0$ $v(w) = \frac{1}{n(w)} \sum_i n(v_i) \left(v(v_i) + (m(v_i) + 1 - m(w))^2 \right)$

Table B1: Recurrence relations for GDG-related metrics computation. w is the parent and the v_i are the children. The mean and variance metrics recurrence relations use formulas for combined (pooled) mean and variance of multiple sample sets.

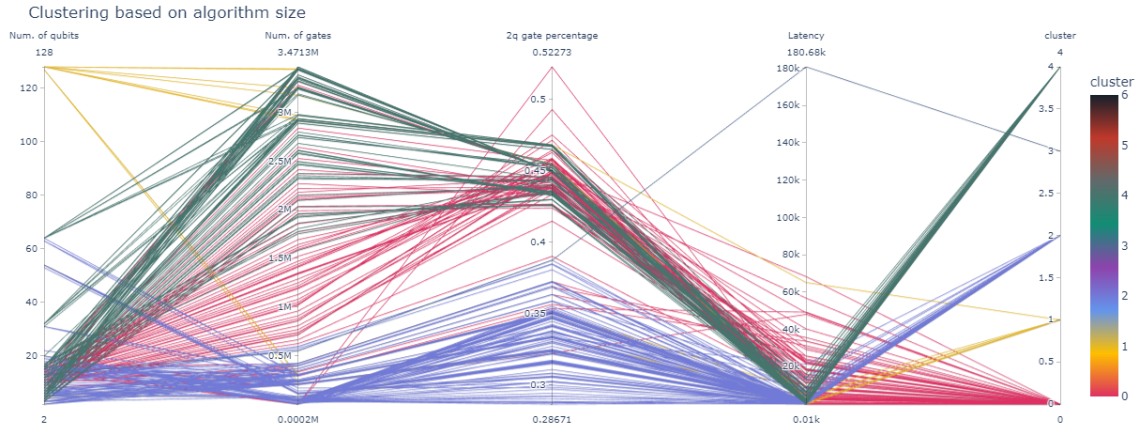


Figure C1: Clustering of quantum circuits based on size-related parameters.

our selection process. An illustration of a cluster and its sub-clusters is provided in Figs. C1 and C2 for reference.

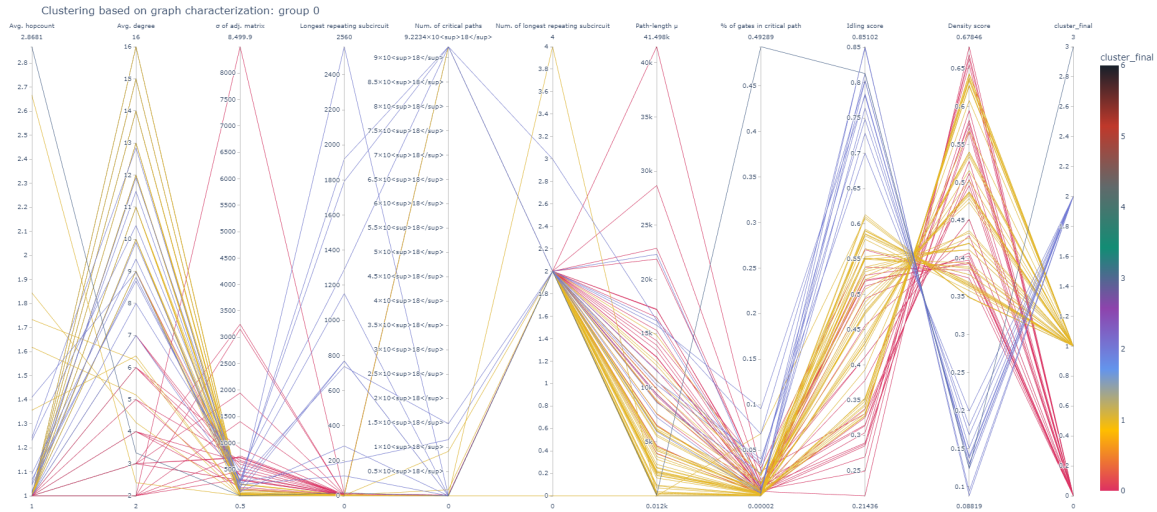


Figure C2: Sub-clustering of quantum circuits of cluster 0 (Fig. C1) based on other structural parameters.

Appendix D. Software availability

The online GitHub repository <https://github.com/QML-Group/QuantumCircuitProfiling> contains the following:

- (i) Benchmarks QASM files;
- (ii) Code for extracting all circuit parameters and clustering together with prerequisites;

- (iii) Code for simulations for different compilers and architectures;
- (iv) Tables containing results: circuit parameters and compilation for all selected benchmarks;
- (v) Tables containing final clusters of benchmarks; and
- (vi) Plots of other extracted results.